8-9-2006

AgSwe1p Regulates Mitosis in Response to Morphogenesis and Nutrients in Multinucleated Ashbya gossypii Cells

Hanspeter Helfer
University of Basel Biozentrum

Amy S. Gladfelter
Dartmouth College

Molecular Biology of the Cell
Vol. 17, 4494–4512, October 2006

AgSwe1p Regulates Mitosis in Response to Morphogenesis and Nutrients in Multinucleated *Ashbya gossypii* Cells[D] [V]

Hanspeter Helfer* and Amy S. Gladfelter*†

*University of Basel Biozentrum, Molecular Microbiology, 4056 Basel, Switzerland; and †Department of Biology, Dartmouth College, Hanover, NH 03755

Submitted March 21, 2006; Revised July 12, 2006; Accepted July 31, 2006
Monitoring Editor: Kerry Bloom

Nuclei in the filamentous, multinucleated fungus *Ashbya gossypii* divide asynchronously. We have investigated what internal and external signals spatially direct mitosis within these hyphal cells. Mitoses are most common near cortical septin rings found at growing tips and branchpoints. In septin mutants, mitoses are no longer concentrated at branchpoints, suggesting that the septin rings function to locally promote mitosis near new branches. Similarly, cells lacking AgSwe1p kinase (a Wee1 homologue), AgHsl1p (a Nim1-related kinase), and AgMih1p phosphatase (the Cdc25 homologue that likely counteracts AgSwe1p activity) also have mitoses distributed randomly in the hyphae as opposed to at branchpoints. Surprisingly, however, no phosphorylation of the CDK tyrosine 18 residue, the conserved substrate of Swe1p kinases, was detected in normally growing cells. In contrast, abundant CDK tyrosine phosphorylation was apparent in starving cells, resulting in diminished nuclear density. This starvation-induced CDK phosphorylation is AgSwe1p dependent, and overexpressed AgSwe1p is sufficient to delay nuclei even in rich nutrient conditions. In starving cells lacking septins or AgSwe1p negative regulators, the nuclear density is further diminished compared with wild type. We have generated a model in which AgSwe1p may regulate mitosis in response to cell intrinsic morphogenesis cues and external nutrient availability in multinucleated cells.

INTRODUCTION

Multinucleated cells are common throughout the biosphere. Filamentous, pathogenic fungi, metastasizing tumor cells, and the cells of the musculoskeletal and blood systems of mammals are examples of the diverse types of cells that contain many nuclei in one cytoplasm. In some cases these cells are produced from specialized cell cycles in which nuclear division occurs without cell division leading to large syncytia. For fungi, multinucleated cells may extend over hundreds of meters so that different regions of a single cell experience dramatically different microenvironments.

Mitosis in multinucleated cells can occur either in a coordinated, synchronous manner where all nuclei divide simultaneously or asynchronously where individual nuclei divide independently in time and space. Synchronous, parasynchronous, and asynchronous patterns of mitosis are observed in syncytial cells, and the different modes of nuclear division bring different potential advantages to cells (Nygaard *et al.*, 1960; Clutterbuck, 1970; Gladfelter *et al.*, 2006). In synchronous division, nuclei in distant regions of the cell can be coordinated, and a cell can globally respond to a signal or stimulus with a limited spatial distribution. Furthermore, synchronous mitoses such as those observed in *Aspergillus nidulans* tip compartments are coordinated with morphogenesis such as tip growth and septation (Harris and Momany, 2004). In asynchronous division, the cell can restrict mitosis to particular nuclei, providing a more local and spatially controlled response to a signal.

Asynchronous or local control of mitosis, which is observed in several filamentous fungi including *Neurospora crassa* and *Ashbya gossypii*, may enable cells to target both growth and nuclear division into nutrient-rich regions, while arresting these processes in areas of the cell lacking sufficient resources (Minke *et al.*, 1999; Freitag *et al.*, 2004; Gladfelter *et al.*, 2006). Additionally, asynchronous control of mitosis may allow cells to directly link morphogenesis programs, such as branching patterns and septal positioning, to nuclear division. Thus external triggers such as nutrients and/or internal signals involving cell shape could spatially direct asynchronous mitosis in multinucleated cells.

In uninucleated *Saccharomyces cerevisiae* cells, cell shape (proper bud formation) is tightly coordinated with nuclear division through a set of cell cycle regulatory proteins that are anchored to the septin scaffold at the mother-bud neck (Kellogg, 2003; Lew, 2003). The septins are conserved filament forming proteins that assemble into heteromeric complexes with diverse functions in eukaryotes, including cytokinesis, morphogenesis, and secretion (Gladfelter *et al.*, 2001; Longtine and Bi, 2003). When bud formation is delayed due to defects in the actin cytoskeleton or if the septin scaffold itself is perturbed, then the intrinsically unstable Swe1p kinase (Wee1 homologue) is stabilized and translocates to the nucleus where it can inhibit the cyclin-dependent kinase/Clb (CDK), Cdc28/Clb2p, through phosphorylation of the tyrosine 19 residue on Cdc28p (Sia *et al.*, 1996; McMillan *et al.*, 1998; Sia *et al.*, 1998; McMillan *et al.*, 1999a, 1999b). This inhibitory phosphorylation provides a G2-delay for cells to recover proper morphogenesis before mitosis, ensuring aberrant binucleate cells do not form in the absence of budding. On restoration of budding or adaptation, the Tyr19

This article was published online ahead of print in *MBC in Press* (http://www.molbiolcell.org/cgi/doi/10.1091/mbc.E06–03–0215) on August 9, 2006.

[D] [V] The online version of this article contains supplemental material at *MBC Online* (http://www.molbiolcell.org).

Address correspondence to: Amy Susanne Gladfelter (Amy.Gladfelter@Dartmouth.edu).

Table 1. *A. gossypii* strains used in this study

Strain	Relevant genotype	Source
wt	*leu2*Δ *thr4*Δ	Altmann-Johl and Philippsen (1996)
AgH4-GFP	pAG-H4-GFP-KanMX6 [*AgHHF1-GFP-GEN3*], *leu2*Δ *thr4*Δ	Alberti-Segui *et al.* (2001)
AgHPH05	pAGHPH002 *[AgSEP7-GFP-GEN3], leu2*Δ *thr4*Δ	This study
AgHPH06	pAGHPH003 *[AgSEP7-GFP-NAT1], leu2*Δ *thr4*Δ	This study
AgHPH07	Ag*SEP7-GFP-GEN3, leu2*Δ *thr4*Δ	This study
AgHPH08	Ag*SEP7-GFP-NAT1, leu2*Δ *thr4*Δ	This study
AgHPH09	Ag*SEP7-GFP-NAT1,* pAG-H4-GFP-KanMX6 *[AgHHF1-GFP-GEN3], leu2*Δ *thr4*Δ	This study
AgHPH10	Ag*cdc3*Δ*::GEN3,* Ag*SEP7-GFP-NAT1, leu2*Δ *thr4*Δ	This study
AgHPH14	Ag*cdc10*Δ*::GEN3,* Ag*SEP7-GFP-NAT1, leu2*Δ *thr4*Δ	This study
AgHPH15	Ag*cdc12*Δ*::GEN3,* Ag*SEP7-GFP-NAT1, leu2*Δ *thr4*Δ	This study
hsl1ΔNAT1	Ag*hsl1*Δ*::NAT1, leu2*Δ *thr4*Δ	This study
ASG41	Ag*HSL7-GFP-GEN3, leu2*Δ *thr4*Δ	This study
AgHPH19	Ag*cdc12*Δ*::NAT1,* Ag*HSL7-GFP-GEN3, leu2*Δ *thr4*Δ	This study
AgHPH20	Ag*hsl1*Δ*::NAT1,* Ag*HSL7-GFP-GEN3, leu2*Δ *thr4*Δ	This study
AgHPH21	Ag*hsl7*Δ*::GEN3, leu2*Δ *thr4*Δ	This study
AgHPH22	Ag*mih1*Δ*::NAT1, leu2*Δ *thr4*Δ	This study
AgHPH23	Ag*mih1*Δ*::GEN3, leu2*Δ *thr4*Δ	This study
ASG35	Ag*swe1*Δ*::NAT1, leu2*Δ *thr4*Δ, *AgSPC42-GFP-GEN3+AgSPC42*	This study
AgHPH24	Ag*swe1*Δ*::GEN3, leu2*Δ *thr4*Δ	This study
AgHPH25	Ag*cdc3*Δ*::GEN3,* Ag*mih1*Δ*::NAT1, leu2*Δ *thr4*Δ	This study
AgHPH26	Ag*cdc10*Δ*::GEN3,* Ag*mih1*Δ*::NAT1, leu2*Δ *thr4*Δ	This study
AgHPH27	Ag*cdc12*Δ*::GEN3,* Ag*mih1*Δ*::NAT1, leu2*Δ *thr4*Δ	This study
AgHPH28	Ag*hsl1*Δ*::NAT1,* Ag*mih1*Δ*::GEN3, leu2*Δ *thr4*Δ	This study
AgHPH29	Ag*hsl1*Δ*::GEN3,* Ag*mih1*Δ*::NAT1, leu2*Δ *thr4*Δ	This study
AgHPH30	Ag*hsl7*Δ*::GEN3,* Ag*mih1*Δ*::NAT1, leu2*Δ *thr4*Δ	This study
AgHPH31	Ag*swe1*Δ*::GEN3,* Ag*mih1*Δ*::NAT1, leu2*Δ *thr4*Δ	This study
AgHPH32	Ag*SWE1-13myc-GEN3, leu2*Δ *thr4*Δ	This study
AgHPH34	pAGHPH006 *[AgSWE1-GFP-NAT1], leu2*Δ *thr4*Δ	This study
AgHPH35	Ag*cdc28*Δ*::NAT1, leu2*Δ *thr4*Δ	This study
AgHPH36	Ag*cdc28Y18F-GEN3, leu2*Δ *thr4*Δ	This study
AgHPH37	pAGHPH008 *[GEN3-*P_{ScHIS3}*-AgSWE1], leu2*Δ *thr4*Δ	This study
AgHPH38	pAGHPH009 *[GEN3-*P_{ScHIS3}*-AgSWE1-6HA], leu2*Δ *thr4*Δ	This study
AgHPH39	pAGSWE1HANAT1 *[AgSWE1-6HA-NAT1], leu2*Δ *thr4*Δ	This study

With the exception of plasmidic strains (square brackets) and ASG35, all analyzed mycelia were homokaryotic (all nuclei have same genotype). This was obtained either by sporulating homokaryotic strains or by applying selective pressure during germination.

phosphorylation is reversed by the phosphatase Mih1p (Cdc25 homologue), which promotes mitotic entry. Swe1p is then directed to the neck and phosphorylated by kinases, including the CDKs, Cla4p (PAK) and Cdc5p (Polo-like kinase; Asano *et al.*, 2005; Sakchaisri *et al.*, 2004; no. 6325). Neck localization of Swe1p is mediated by Hsl7p, which is anchored to the septins by Hsl1p (Barral *et al.*, 1999; Shulewitz *et al.*, 1999; Longtine *et al.*, 2000; Cid *et al.*, 2001). After phosphorylation, Swe1p is targeted for ubiquitin-mediated degradation in the proteasome (Sia *et al.*, 1998). Thus the septin scaffold functions to coordinate bud morphogenesis and nuclear progression by regulating the abundance of Swe1p, and collectively these factors make up the budding yeast "morphogenesis checkpoint."

The homologues of all of these factors including the septins, Swe1p, Hsl1p, Hsl7p, and Cdc28p are present with varying degrees of homology in the genome of the multinucleated, filamentous fungus *A. gossypii*. This ascomycete diverged from a common ancestor of *S. cerevisiae* over 100 million years ago and shares many similar genomic features with this budding yeast yet never reproduces by budding and rather is exclusively found in a filamentous, multinucleated hyphal form (Dietrich *et al.*, 2004). Given the absence of budding yet the conservation of all factors involved in the morphogenesis checkpoint, we speculated that septins may link morphogenesis to the nuclear division cycle in this filamentous fungus by directing where mitosis takes place in the cell. Thus here we have investigated if and how the septins may spatially direct mitoses in multinucleated hyphae.

We show here that the septin proteins assemble into rings in areas where growth and mitoses are most frequent, at branchpoints and growing tips in multinucleated *A. gossypii* cells. This spatial pattern of nuclear division requires septins and involves regulation of the AgSwe1p kinase in response to internal cues for branching. Additionally, AgSwe1p also regulates nuclear progression in response to external nutrient status through inhibitory phosphorylation of the CDK. We propose that this dual role for AgSwe1p may be used to facilitate a spatially controlled reaction to limited nutrient availability in the natural world.

MATERIALS AND METHODS

A. gossypii Methods, Media, and Growth Conditions

A. gossypii media, culturing, and transformation protocols are described in Wendland *et al.* (2000) and Ayad-Durieux *et al.* (2000). *A. gossypii* strains used here are listed in Table 1. To test the influence of high culture density, 10–20 ml of full medium was densely inoculated with spores (10× higher spore inoculum), and the cultures were grown until vacuoles were clearly observable by phase contrast microscopy. For all other conditions, 50–100 ml of full medium were inoculated at low density and regularly controlled for the absence of visible vacuoles, and fresh medium was added 1–2 h before taking samples or exposing the cultures to conditions of potential stress. Nocodazole

Table 2. Plasmids used in this study

Plasmid	Vector	Relevant insert	Source
pUC19	—	—	
pRS416	—	—	Sikorski and Hieter (1989)
pGEN3	pAF100	*GEN3*	Wendland *et al.* (2000)
pAg13-myc	pGEN3	*13myc-GEN3*	Gladfelter *et al.* (2006)
pGUG	pGEN3	*GFP-GEN3*	Knechtle *et al.* (2003)
pUC19NATPS	pUC19	*NAT1*	D. Hœpfner
pGUC	pGUG	*GFP-NAT1*	This study
pAG-H4-GFP-KanMX6	pAG1552	Ag*HHF1-GFP-GEN3*	Alberti-Segui *et al.* (2001)
pAG4401	pRS416	Ag*SEP7*	C. Mohr (1995)
pAGHPH002	pAG4401	Ag*SEP7-GFP-GEN3*	This study
pAGHPH003	pAG4401	Ag*SEP7-GFP-NAT1*	This study
pUCHPH002	pUC19	Ag*SEP7-GFP-GEN3*	This study
pUCHPH003	pUC19	Ag*SEP7-GFP-NAT1*	This study
pAGHPH004	pRS416	Ag*SWE1*	This study
pAGHPH005	pAGHPH004	Ag*SWE1-13myc-GEN3*	This study
pAGHPH006	pAGHPH004	Ag*SWE1-GFP-NAT1*	This study
pRS416CDC28GEN3	pRS416	Ag*CDC28-GEN3*	This study
pAGHPH007	pRS416Cdc28GEN3	Ag*cdc28Y18F-GEN3*	This study
pAGrPXC	YCplac111	PSc*HIS3-CFP*	D. Hœpfner
pAGHPH008	pAGHPH004	*GEN3*-PSc*HIS3*-Ag*SWE1*	This study
pAGSWE1HANAT1	pAGHPH004	Ag*SWE1-6HA-NAT1*	This study
pAGHPH009	pAGHPH008	*GEN3*-PSc*HIS3*-Ag*SWE1-6HA*	This study

pAG plasmids are based on the pRS416 vector (Sikorski and Hieter, 1989).

stocks for the arrest and release experiment were 3 mg/ml in DMSO and were used at a final concentration of 15 μg/ml (Sigma, St. Louis, MO). Hydroxyurea was directly added to the cultures to a final concentration of 50 mM. Rapamycin stocks (LC Laboratories, Woburn, MA) were 1 mg/ml in 90% EtOH and 10% Tween-20 and were used at a final concentration of 200 nM (Loewith *et al.*, 2002). To simulate the starvation response, low-density cultures were washed twice and resuspended in 40 mM MOPS, pH 7.0, 137 mM KCl. To test the lack of certain nutrients, different media based on Ashbya Synthetic Dextrose (ASD) medium were used: 1.70 g/l YNB without amino acids and without ammonium sulfate (Difco, Detroit, MI), 0.69 g/l CSM-LEU (BIO 101, Carlsbad, CA), 1.00 g/l Asn, 0.01 g/l adenine, 1.00 g/l myo-inositol, 20 g/l glucose, and 50 mM MOPS, pH 6.5.

Plasmid and Strain Construction

All DNA manipulations were carried out according to Sambrook (2001) with DH5aF′ as host (Hanahan, 1983). Plasmids used here are listed in Table 2. PCR was performed using standard methods with different polymerases from Roche (Basel, Switzerland), Amersham Biosciences (Little Chalfont, Buckinghamshire, United Kingdom), or GenScript (Piscataway, NJ). Oligos were synthesized at MWG (Ebersberg, Germany) or Microsynth (Switzerland), and all restriction enzymes came from New England Biolabs (Beverly, MA) or Roche. Oligonucleotide primers are listed in Table 3. Plasmid isolation from yeast and sequencing were performed as described in Schmitz *et al.* (2006).

A. gossypii deletion mutants were generated using the PCR-based, one-step gene targeting approach with nonhomologous selection markers (McElver and Weber, 1992; Baudin *et al.*, 1993; Wach, 1996; Wendland *et al.*, 2000). For G418 resistance, the deletion cassettes were amplified off the pGEN3 template using "gene name"–S1/S2 primer pairs. ClonNAT (Werner Bioagents, Jena, Germany) resistance was obtained using pUC19NATPS as template. N*S1/N*S2 primer pairs were used for expression of the NAT1 resistance module under the control of the promoter and terminator of the targeted gene. NS1/NS2 primer pairs lead to NAT1 expression under the control of the ScPDC1 promoter and terminator. Correct integration was verified by analytical PCR with oligonucleotides "gene name"-(N)G1, -(N)G4, -I1/I2 (genomic) and G2.1, G3, V2PDC1P, V3PDC1T, V2*NAT1, and V3*NAT1 (marker). To exclude phenotypes by random mutations, at least two independent transformants were characterized for each deletion. Transformation of multinucleate mycelium leads to heterokaryotic cells, which contain a mixture of transformed and wild-type (wt) nuclei, and usually do not display an apparent phenotype. For subsequent analysis, homokaryotic mycelium was obtained by isolating and growing single spores. To evaluate phenotypes of lethal mutants or mutants with sporulation deficiency, spores from heterokaryotic mycelium were germinated and analyzed under selective conditions. For the creation of the double deletion strains AgHPH29 and AgHPH31, at least three homokaryotic isolates bearing the first deletion that were phenotypically not distinguishable were tested for correct integration of both ends of the deletion cassette and absence of the wt gene using verification PCR. One of these isolates was grown and transformed with the deletion cassette for the second gene, using a different selection marker. If no homokaryotic mycelium of the first deletion mutant was available yet (for creation of AgHPH27 and AgHPH28), spores from heterokaryotic mycelium were grown under selection and transformed with the second deletion cassette. In both cases, three primary transformants resulting from the second transformation were isolated. Verification PCR was used to test correct integration of both deletion markers. To test absence of both wt genes, homokaryotic mycelium was isolated from the double deletion mutants and verified using PCR.

A C-terminal fusion of GFP to AgSep7p was obtained by amplifying pGUG and pGUC with S7-G-S1 and S7-G-S2 or S7-G-S1, and S7-G-CS2, respectively. To generate Ag*SEP7-GFP-NAT1*, the pGUC cassette was first constructed by digesting pGUG with BglII and BamHI and ligating the gel-purified 1026-base pair fragment into the dephosphorylated pUC19NATPS vector, which was linearized with BamHI.

The S7-G–S1 primer was designed with homology to the C-terminal region of *AgSEP7* before the stop codon. The PCR products were each transformed together with pAG4401, containing *AgSEP7,* into the *S. cerevisiae* strain CEN.PK2 (Entian and Koetter, 1998) for in vivo recombination. The resulting plasmids pAGHPH002 and pAGHPH003 were purified and transformed into *A. gossypii* wt cells, leading to the strains AgHPH05 and AgHPH06. For integration into the genome, the two constructs were first subcloned into pUC19 to eliminate ARS activity. pUC19 was opened with SalI and XbaI, *AgSEP7-GFP-GEN3* was excised from pAGHPH002 with EcoRI, and SphI and pAGHPH003 was cut with XhoI and SpeI to extract *AgSEP7-GFP-NAT1.* The fragments were gel-purified and separately ligated into the dephosphorylated pUC19 fragment to produce pUCHPH002 and pUCHPH003. The cassettes were excised with EcoRI and transformed into *A. gossypii* wt cells, giving rise to AgHPH07 and AgHPH08.

To generate ASG41 (*AgHSL7-GFP-GEN3*), the oligos Hsl7-S1 and Hsl7-S2 (with homology to the C-terminus of *AgHSL7*) were used with the template pGUG to generate the PCR product that was used to directly transform *A. gossypii* cells.

To make the nonphosphorylatable Y18F mutation of *AgCDC28,* the plasmid pAGHPH007 was created using in vivo gap repair in *S. cerevisiae*. First, Ag*CDC28* was amplified from genomic DNA using oligos Cdc28aIEcoR1 and Cdc28aIIBamH1, with homology upstream of Ag*CDC28* including the promoter region and limited downstream sequence. This PCR fragment was purified and digested with EcoRI and BamHI, sites present in the oligos, to clone it into pRS416 that was opened with these same enzymes. The entire Ag*CDC28* ORF was sequenced to confirm that PCR did not introduce point mutations. pRS416*CDC28GEN3* was cut with XhoI at two sites, one being 23 base pairs upstream of Y18, the other being located in the pRS416 backbone. The resulting fragments were cotransformed into the *S. cerevisiae* strain DHD5 (Arvanitidis and Heinisch, 1994) together with the annealed oligonucleotides

Table 3. Oligonucleotide primers used in this study

Primer	Sequence 5′–3′
S7-G-S1	CAATTTGCTAGTGATGGATATGCTTCCCGCGCAACAGGCCAGGTACAAggtgcaggcgctggagctg
S7-G-S2	GCATTGACCCTCGGGCAAAGGATAAGATATATAGTTAGAAGATGTTagggacctggcacggagc
S7-G-CS2	GCATTGACCCTCGGGCAAAGGATAAGATATATAGTTAGAAGATGTTgattacgccaagcttgcatgcc
S7-G-G1	GCCAAACAACAAAAGCTGGAG
S7-G-G4	GTGCCCAGCATTTCATGGAAC
S7-G-CG4	GCCGTACGCGATCTGGCAATAGATGCGACATCC
Hsl7-S1	GACAAATACCACTGAGTTACACAATATTGGCGGTCATGCCTACATGATTAAATTGggtgcaggcgctggagctg
Hsl7-S2	GTATGCGGAAGCATAAATAGAAATGTTGCTTTTATGTTAGCATAGCGCGAagggacctggcacggagc
C3-S1	GCGTTATACAGGACCTACACACGTACAGGACTACCAAATCAGAACAAGCgctagggataacagggtaat
C3-S2	GTGACAATAATCAAGACAAATAGACTGTTTTTTTCGATTGCGGGTAGCaggcatgcaagcttagatct
C3-G1	AAACAGCGGACCACCACAAC
C3-G4	GACTTCTGCTGGCGGATACC
C3-I1	CCCACGCAGAGCAAATTGAG
C10-S1	GTTCACTCAAAGGAGCGCAAACAGCACTACTCATCCGAAACACGTTTACACCAGTTCCgctagggataacagggtaat
C10-S2	GTTTGAGTACCCTCAATATTGGTAGATCTGGTGACTTTTAAAAAGTTAGGGGTTATTCaggcatgcaagcttagatct
C10-G1	CTCCGCCTCCTTAGGAACTG
C10-G4	TGTCGCTTACTGCAGGCCATC
C10-I1	GTGTCCACGATGTGCTTCTC
C12-S1	CCTCAGACGCAAGGGCAACAGTGCAATAGGTGTGTTTGGTAACTTCgctagggataacagggtaat
C12-S2	GCTGATCTGTCATTTCTAGTTGGTTCCACTACTGAAGATGATACGGaggcatgcaagcttagatct
C12-NS1	CCTCAGACGCAAGGGCAACAGTGCAATAGGTGTGTTTGGTAACTTCccagtgaattcgagctcgg
C12-NS2	GCTGATCTGTCATTTCTAGTTGGTTCCACTACTGAAGATGATACGGtacgccaagcttgcatgcct
C12-G1	GATTATGTCCGCGTCGCAC
C12-G1.2	GCGGCTTCCAAAGGACAAC
C12-G4	TGGCACGGCTGCATCTTTAC
C12-I1	GCTGCCTCCGATTCTGATTC
HSL1-NS1	GCAGCACAGAGTGTAAGAAACCACAGAGGAGGATGACCGCAGGGCAccagtgaattcgagctcgg
HSL1-NS2	CATTTGCAGCATTCTCCTTTGCTTTAATGAGTGCCTCAATGTCTGtacgccaagcttgcatgcct
HSL1-NG1	GCTACTATTGAAGGTTGCAGC
HSL1-NG4	CTTCTTATGTCGGCGTACCTAGTG
HSL1-I2	CGCAGCAACCAAGGTGTCTG
HSL1-S1.2	GTGTAAGAAACCACAGAGGAGGATGACCGCAGGGCACCGAGACGAGAGgctagggataacagggtaat
HSL1-S2.2	CTCATCACTTCTTCCCTTTTGCTTGACAGACACCTTGGTTGCTGCGCTATaggcatgcaagcttagatct
HSL1-G1.2	TGCAGCCCGTTTCCAACTAC
HSL1-S4.2	GAGTGCCTCAATGTCTGTG
HSL7-S1.2	GTATCAAGGGCCACGGGGTGCTAGAAGGCGCTGCGTACCGGGGAGAAGTACgctaggataacagggtaat
HSL7-S2.2	CGGTCGGAAGTGATCATGAGAAGTGAAATTCAGTTGCCACAGTGCTAGCCaggcatgcaagcttagatct
HSL7-G1.2	GTTTGTTTACTGCGGTGGTC
HSL7-G4.2	GTTAGCATAGCGCGAACA
HSL7-I2.2	ACCAGGTCGAAGAAACAC
MIH1-S1	CAAAAAAAAGCCTACTTTCTCTACTTAATAGTGTTTACTCGAGCACgctagggataacagggtaat
MIH1-S2	CTTAAGAGTCGTTGTCCTCCTCCTTGACGATCTCTGGGAAAAGCCaggcatgcaagcttagatct
MIH1-NS1	CAAAAAAAAGCCTACTTTCTCTACTTAATAGTGTTTACTCGAGCACccagtgaattcgagctcgg
MIH1-NS2	CTTAAGAGTCGTTGTCCTCCTCCTTGACGATCTCTGGGAAAAGCCtacgccaagcttgcatgcct
MIH1-G1	CAGGCGCAGAAGTCGTTAC
MIH1-G4	GACGCGCAGTTGTTGCTTC
MIH1-I1	CCTCTGTCTCGCTCTTTCG
SWE1-NS1	CAAGGTACCAGCGGCAAGCGCGCAGAGAAGACACAGACTAAGAATGccagtgaattcgagctcgg
SWE1-NS2	CCTTATGGTGGCCGGGGAGCGCGATATGCGCCGAACATGCATTCTGtacgccaagcttgcatgcct
SWE1-S1	CAAGGTACCAGCGGCAAGCGCGCAGAGAAGACACAGACTAAGAATGgctagggataacagggtaat
SWE1-S2	CCTTATGGTGGCCGGGGAGCGCGATATGCGCCGAACATGCATTCTGaggcatgcaagcttagatct
SWE1-B1	gcgaattcCGCCTCAGCTTGATCATCGTCAC
SWE1-B2	cgggatccATCGGTATCTGCCGAACACAATGC
SWE1-G-S1	CCATCATCCAAGAAGACGACTTTGGTCCCAAGCCGGAGTTCTTCAGCggtgcaggcgctggagctg
SWE1-G-NS2	CGCACGTTCACTTGTAGCCGAGAAGCCCCTTATGGTGGCCGGGGAGgattacgccaagcttgcatgcc
SWE1-MS1	CCATCATCCAAGAAGACGACTTTGGTCCCAAGCCGGAGTTCTTCAGCcggatccccgggttaattaacggtgaa
SWE1-MS2	CGCACGTTCACTTGTAGCCGAGAAGCCCCTTATGGTGGCCGGGGAGcactagtggatctgatatcagatctgg
AgSWE1 G1	CTCACCTCGAGGCCACTCCGTGTGAGG
SWE1-G-G1	CATCGCGCCGGAAATCATC
AgSWE1 G4	GCAGAGACGCTCAGAGAGATTCCCATTG
AgSWE1 I	GCGACTGAGAGCGATCCGATATTAAGG
SWE1-SH1	AGGAGAAGGGCATACAGTTCCCCACGAATTTCGGCATAGAAAGGCgaattcaggcatgcaagcttagatct
SWE1-SH2	GTTCAGAAACGGCGACTCGCGCAGCGCTGCCATGCTGTCGTGCCGGAGCGTCATggatccccgggtaccgagctctttg
MH1	GTATTACCCTGTTATCCCTAGCATTCTATTACTCTTGGCCTCC
MH2	GGAGGCCAAGAGTAATAGAATGCTAGGGATAACAGGGTAATAC
HISP-HG2	TTTCCACCTAGCGGATGAC
SWE1-HG1	ATGGACGCCACAGGTTATCTC

Continued

Table 3. *Continued*

Primer	Sequence 5′–3′
CDC28-N*S1	ACTCCCTATGTACCCCACGGGCACGGGCCCATAAACCGGCAAAAAACGCGCCTGCGACAGAAAATTTTGTG TACCTCTACCACCAGCACCTCatgggtaccactcttgacgac
CDC28-N*S2	AGCAGCGCAATCTACATGCAAACGCGGTACAGCACCAGCGCTACTATTTATACCACCTACGTAGCTGCC TGTTCTGGCAGCGAGCGGCCTAggggcagggcatgctcatgtag
CDC28-N*G1	TGCTGACGATGGGCTCCTTC
CDC28-N*G4	TGTGGACCCTCCCAGTTACC
CDC28-IB	TGCACATTTCGGCGAAGATG
CDC28-G1.2	AGGAGTGACCTCCTCTACAG
CDC28-IA-Y18	GAACGTATGGTGTCGTCTAC
CDC28-Y18F-A	CCCTCATGAGCGATCTCACCAACTACAAGCGCTTGGAAAAAGTCGGTGAAGGTACCTTCGG GGTTGTTTATAAAGCGGTTG
CDC28-Y18F-B	CGCCACGATGCGCTGCCCATGCCGCAGGTCAACCGCTTTATAAACAACCCCGAAGGTACCTT CACCGACTTTTTCCAAGC
CDC28-glue-A	GGGCGAATTGGGTACCGGGCCCCCCCTCGAGGTCGACGGTATCGATAAGC
CDC28-glue-B	GCTTATCGATACCGTCGACCTCGAGGGGGGGCCCGGTACCCAATTCGCCC
CDC28-Y18F-IA	GGTACCTTCGGGGTTGTTTA
CDC28-G4.2	ATGTGCGCGAGGCTCTTTC
Cdc28aIEcoRI	CATAGAATTCACTTCCGTGCCTGGGTGCAGCAGCATCGGCTTC
Cdc28aIIBamHI	GTTCGGATCCTGACGATGGGCTCCTTCGACGGCCTGTTG
Swe1F1	CCATCATCCAAGAAGACGACTTTGGTCCCAAGCCGGAGTTCTTCAGCAAAACGACGGCCAGTGAATTCG
Swe1F2	CGCACGTTCACTTGTAGCCGAGAAGCCCCTTATGGTGGCCGGGGAGACCATGATTACGCCAAGCTTGC
G2.1	tgcctccagcatagtcgaag
G3	tcgcagaccgataccaggatc
V2PDC1P	gaacaaacccaaatctgattgcaaggagagtgaaagagcctt
V3PDC1T	gaccagacaagaagttgccgacagtctgttgaattggcctg
V2*NAT1	gtgtcgtcaagagtggtacc
V3*NAT1	acatgagcatgccctgcccc
GG2	catcaccttcaccctctccac
MYCI	cgagtccgttcaagtcttcttctgag

Lowercase letters are regions of homology to the cassette containing a selectable marker. Underlined letters represent intragenic replacements (alternative codons, point mutations).

CDC28-Y18F-A/CDC28-Y18F-B and CDC28-glue-A/CDC28-glue-B for in vivo recombination. The pair CDC28-Y18F-A/CDC28-Y18F-B overlapped the first XhoI site and contained the Y18F replacement flanked by a total of 15 silent mutations to improve the fidelity of subsequent genomic integration into *A. gossypii.* The second XhoI site was overlapped by the pair CDC28-glue-A/CDC28-glue-B, which contained no mutations. The gap-repaired plasmid (pAGHPH007) was isolated and verified by sequencing of the altered regions. pAGHPH007 was digested with EcoRI, BamHI, and PstI and transformed into *A. gossypii* wt cells, resulting in AgHPH36. Correct integration and presence of the altered region was verified by analytical PCR with the oligonucleotides CDC28-IB/CDC28-Y18F-IA (binds to altered sequence, only) and G3/CDC28-G4.2 and CDC28-IB/CDC28-IA-Y18 (binds to wt sequence, only). For additional verification, a fragment containing the altered sequence was amplified using CDC28-G1.2/CDC28-IB and digested with KpnI, which cuts the mutated fragment at two places and the wt fragment at one site, only.

The plasmid carrying *AgSWE1* (pAGHPH004) was generated by amplification of the gene from genomic *A. gossypii* DNA using the primers SWE1-B1 and SWE1-B2, which contain EcoRI and BamHI restriction sites. The fragments were purified, cut and ligated into pRS416. The resulting plasmid was verified to contain no mutations by sequencing.

To C-terminally tag AgSwe1p with GFP or 13-myc, the pGUC or pAG13-myc cassette was amplified with SWE1-G-S1 and SWE1-G-NS2 or SWE1-MS1 and SWE1-MS2, respectively. The resulting PCR products were cotransformed into the *S. cerevisiae* strain DHD5 together with pAGHPH004 for in vivo recombination, giving rise to pAGHPH005 and pAGHPH006. Correct fusion was verified by sequencing. Transformation of the plasmid pAGHPH006 into *A. gossypii* wt cells produced the strain AgHPH34. To obtain AgHPH32, pAGHPH005 was digested with BmgBI and BssHII before transforming it into *A. gossypii* wt cells, leading to genomic integration.

For overexpression of *AgSWE1,* the plasmid pAGHPH008 was constructed: the *ScHIS3* promoter was amplified off pAGrPXC (kindly provided by Dominic Hœpfner) using the primer pair MH1 and SWE1-SH2. The *GEN3* cassette was amplified using the oligonucleotides MH2 and SWE1-SH2 with pGEN3 as template. MH1 and MH2 contained homology to both, the *GEN3* cassette and the *ScHIS3* promoter, generating an overlap between the two PCR products. SWE1-SH1 and SWE1-SH2 added 45-base pair homology to a region upstream of *AgSWE1* START and 54-base pair homology to the very START of *AgSWE1.* The two PCR products were used together as template in a subsequent PCR reaction with the primers SWE1-SH1 and SWE1-SH2. The resulting *GEN3-ScHIS3* cassette was fused in front of *AgSWE1* by in vivo recombination with pAGHPH004 in the *S. cerevisiae* strain DHD5, leading to pAGHPH008. The plasmid was purified and verified by sequencing and transformed into *A. gossypii* wt cells to produce AgHPH37. To C-terminally tag *GEN3-ScHIS3/SWE1* with HA, a 980-base pair fragment carrying the carboxy end of AgSwe1p fused to 6HA was cut out of pAgSWE1-HA-NAT1 using MscI and ScaI. To generate pAgSWE1-HA-NAT1, the Swe1F1 and Swe1F2 oligos, which have homology to the C-terminus of *AgSWE1* and the universal tagging cassette, were used in a PCR reaction with the pN1–6HA (pAGT105-kindly provided by Andreas Kaufmann, University of Basel, Basel, Switzerland) template, and the resulting product was cotransformed into budding yeast cells with the plasmid pAGHPH004. Recombination of the plasmid with the linear PCR fragment resulted in yeast cells resistant to CloNAT. Plasmids were rescued from these resistant yeast strains and correct fusion of *6HA* to *AgSWE1* was verified by restriction digest. pAGHPH008 was opened with MscI and XbaI. T4 DNA polymerase was used to fill the 5′ protruding end generated by XbaI. The dephosphorylated 8910-base pair vector fragment was gel-purified and ligated with the 980-base pair insert to produce pAGHPH009. In frame fusion of the tag was verified by sequencing. Transformation of the plasmid pAGHPH009 into *A. gossypii* wt cells produced the strain AgHPH38.

Protein Extraction and Western Blotting

Cells grown under the desired conditions were collected, washed once with ice-cold PBS containing 1 mM Na_3VO_4 and 1 mM β-glyerolphosphate, and suspended in ice-cold lysis buffer (50 mM Tris-HCl, pH 7.5, 150 mM NaCl, 5 mM EDTA, 1% NP-40, 2 mM sodium pyrophosphate, 1 mM Na_3VO_4, 1 mM β-glycerolphosphate, and Roche complete protease inhibitor cocktail). An equal volume of 0.5-mm glass beads was added to this suspension, and cells were broken by vigorous vortexing during 6 × 30-s intervals in a bead beater at 4°C. Total cellular proteins were separated by SDS-PAGE (12%) and transferred to nitrocellulose membranes (Amersham Biosciences), using standard conditions. Blocking was performed with 5% milk in TBS-Tween-20 (0.1%). For detection of phosphorylated AgCdc28p, rabbit anti-phospho-cdc2(Tyr15) (Cell Signaling, no. 9111) was used at

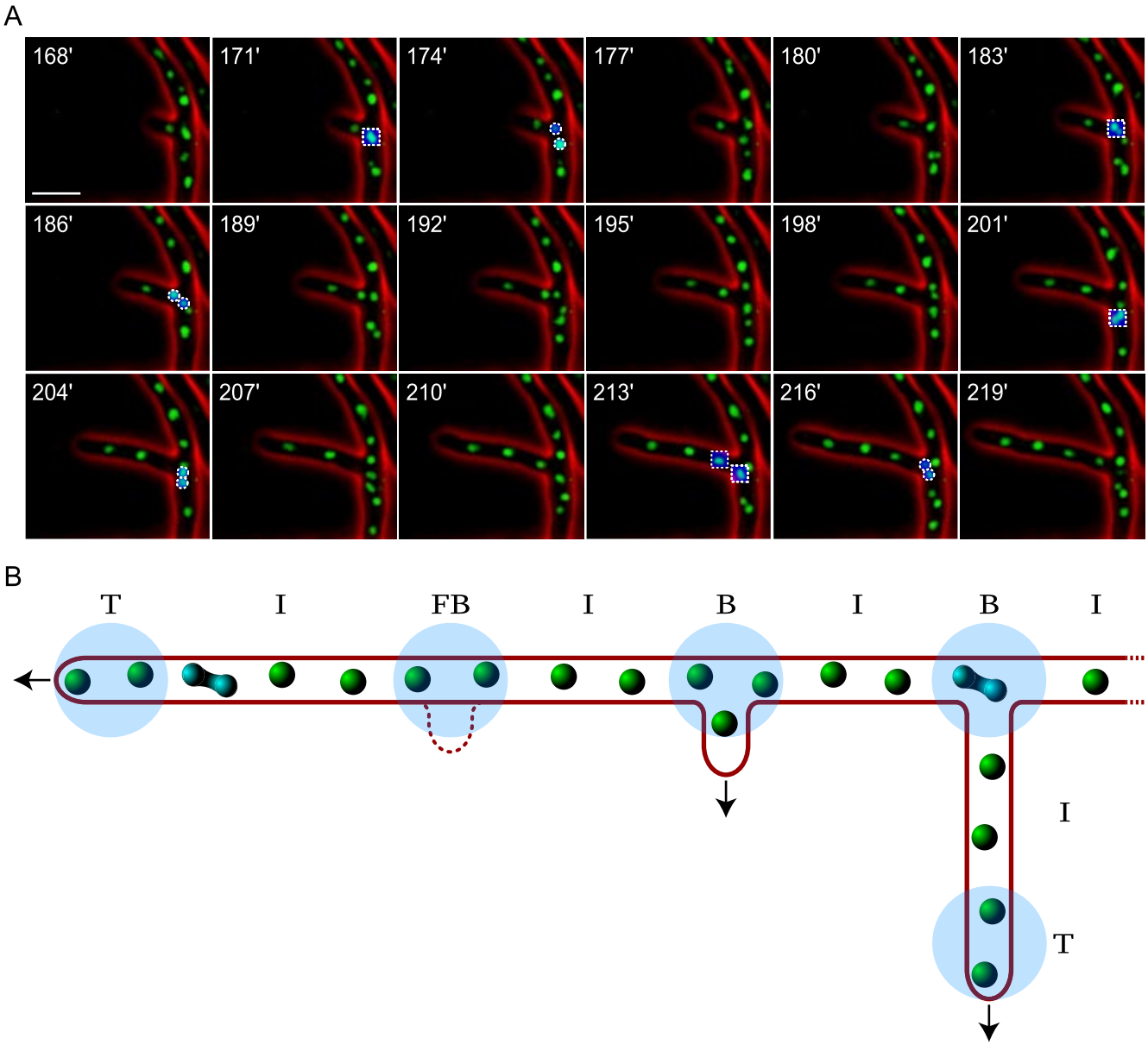

Figure 1. Mitoses are enriched at branching points. (A) AgH4-GFP cells were grown as described in Supplementary Movie 1, and images were collected at 3-min intervals. Cell outlines are in red, nuclei are in green, and mitoses are false-colored blue and labeled with a box just before division and new daughter nuclei are outlined with circles. Bar, 10 μm. (B) Schematic illustrates the method used for scoring the positions of mitoses within the developing mycelium. The closest 10 μm (shaded blue circles) to growing tips were considered as tip region T. B and FB indicate zones of 10 μm (shaded blue circles) around sites of branch formation or future sites of branch formation, respectively. The regions between tips, and branches were scored as interregions 'I'.

1:1000 in TBS, 5% BSA, 0.1% Tween-20, and HRP-anti-rabbit (Cell Signaling, no. 7074) was used at 1:2000 in TBS, 5% milk, 0.1% Tween-20. As positive control for phosphorylated CDK, total cellular proteins were extracted from the *S. cerevisiae* strain DLY5544 (*cdc12-6, GAL/SWE1*), grown in YP 2% sucrose, and induced by adding 2% galactose. For detection of HA-tagged proteins, mouse anti-HA was used at 1:1000 in TBS, 5% BSA, 0.1% Tween-20, and HRP-anti-mouse (Jackson ImmunoResearch, West Grove, PA) was used at 1:1000 in TBS, 5% milk, 0.1% Tween-20. Detection of labeled proteins was performed by using the enhanced chemiluminescence (ECL) detection system (Amersham Biosciences). Either nonspecific cross-reacting bands or bands from Ponceau red staining of the membrane was used for load controls.

Immunofluorescence, Image Acquisition, and Processing

DNA stainings (Hoechst 33342) and immunofluorescence stainings were performed as described previously (Gladfelter *et al.*, 2006). Rabbit anti-ScCdc11p (Santa Cruz Biotechnology, Santa Cruz, CA) was diluted in PBS and used at a 1/10 dilution. Rabbit anti-phospho-cdc2(Tyr15) was used at 1/50 for immunofluorescence. For in vivo observation of mycelium containing GFP-tagged proteins, the cells were grown for 10–12 h in full medium and then washed and resuspended in ASD or MOPS/KCl for observation under the microscope.

The microscopy setup used was the same as described in Hœpfner *et al.* (2000), Knechtle *et al.* (2003), and Gladfelter *et al.* (2006). The following filter sets were used for the different fluorophores: no. 02 for Hoechst, no. 15 for Rhodamine 568 (Carl Zeiss, Thornwood, NY), and no. 4108 for GFP (Chroma Technology, Brattleboro, VT).

For still images, multiple planes with a distance between 0.3 and 0.5 μm in the Z-axis were taken. MetaMorph 4.6r9 software (Universal Imaging, West Chester, PA) was used for ("no-neighbors") 2D-deconvolution. The stacks were flattened into a single plane using stack arithmetic "maximize" command. Outlines of the cells were obtained by doing phase-contrast Z-series. The stacks were passed

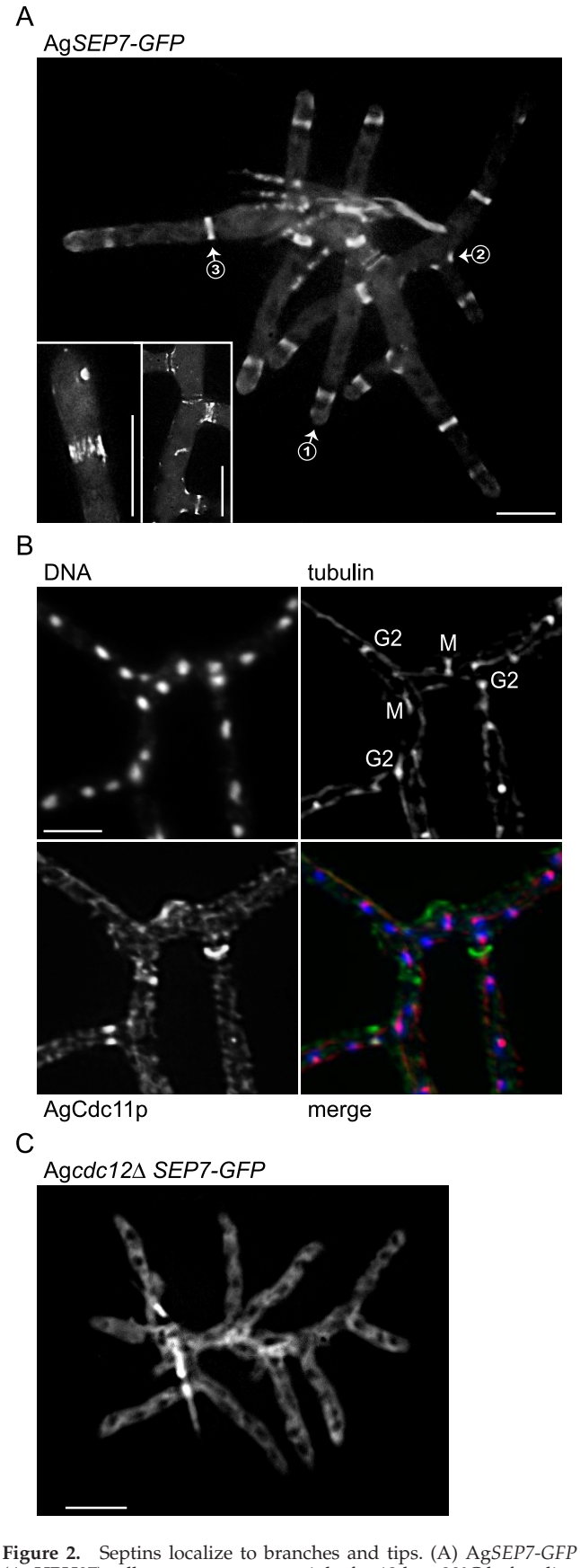

Figure 2. Septins localize to branches and tips. (A) Ag*SEP7-GFP* (AgHPH07) cells were grown overnight for 12 h at 30°C before live imaging. Tip rings (1 and inset, left), branch rings (2 and inset, right) and main hyphal rings (3) are visible. (B) Wild-type cells (*leu2*Δ *thr4*Δ) were grown overnight for 16 h at 30°C and processed for anti-tubulin and anti-Cdc11p immunofluorescence. In overlay, DNA is blue, tubulin is red, and septins are green. (C) Ag*cdc12*Δ*SEP7-GFP* (AgHPH15) cells were grown for 12 h at 30°C and then imaged live. Bars, 10 μm.

through the Metamorph filter "detect edges: Laplace 2" and flattened into a single plane using the stack arithmetic "sum" command. Fluorescent and phase-contrast images were scaled and overlaid using "color align."

Time-lapse images were taken as described in Gladfelter *et al.* (2006) and assembled into movies using QuickTimePro 6.5. Mitotic events in Supplementary Movie 1 were labeled manually using Adobe Photoshop CS.

RESULTS

Mitoses Are Enriched at Branching Points

To investigate if there is spatial control of asynchronous mitosis in multinucleated *A. gossypii* cells, we measured the mitotic index in tips, branchpoints, and regions between these growth areas using several methods. First, we observed cells growing on agar expressing GFP-labeled Histone H4 (Ag*HHF1-GFP*) using time-lapse microscopy to follow nuclear dynamics and morphogenesis over multiple hours in vivo (Supplementary Movie 1). Mitoses were frequently observed near newly emerging branches at the junction between the new branch and the "mother" hypha (Figure 1A). In the frames of the movie shown in Figure 1, mitoses occurred preferentially at the branching site at 171, 183, 201, and 213 min. Mitoses observed near a newly emerging branch are labeled with a box just before division, and new daughter nuclei are then outlined with circles. In 84 total mitoses captured by time lapse, 12% were at hyphal tips (which represent 11% of total hyphal length), 51% were at current or future branching sites (which represent 30% of total hyphal length), and 37% were in the middle of hyphae (a region not near the tip or branching sites that represents 59% of total hyphal length). Thus, there were 1.7 times the number of mitoses at branches than would be expected if mitoses were distributed without respect to location. Additionally, to assay mitotic frequency and position using an alternative method, wt cells were grown in liquid medium and then processed for anti-tubulin immunofluorescence to visualize mitotic spindles. In this case, branchpoints were similarly enriched for mitoses with 45% of mitotic nuclei at these sites, whereas tips hosted 30% of the dividing nuclei and 25% were present in the interregion ($N > 200$ nuclei, presented in graphical form in Figure 4C).

Mitosis could occur in branching sites simply due to cytoplasmic increases that trigger a cell-size cue that promotes mitosis. Alternatively or additionally, there could be positional markers deposited in areas of growth that recruit cell cycle regulators and directly influence the position of mitosis. Notably, we observed when mitoses occur in the absence of branching in the interregion that in many cases a branch later emerged from that spot suggesting that certain regions of a hypha are "marked" to promote mitosis (18% of mitoses, Supplementary Figure 1).

Septins Localize to Branches and Tips and Influence the Position of Mitoses

We speculated that septin proteins may function as a marker directing where nuclei divide and thus localized septin proteins in *A. gossypii*. The *A. gossypii* septins were visualized in living cells using a GFP-tagged septin, AgSep7p-GFP, and by immunofluorescence using an antibody generated against ScCdc11p. In living and in fixed cells, the septins assembled

Table 4. Homologues of the *S. cerevisiae* morphogenesis checkpoint components in *A. gossypii*

Protein	Size (aa)		Identity (%)	Syntenic homolog	Key domains[a]	
	A.g.	S.c.			A.g.	S.c.
Cdc28p	296	298	86	Yes	Protein kinase	Protein kinase
Swe1p	728	819	52	Yes	Protein kinase	Protein kinase
Mih1p	469	554	34	Yes	Phosphatase, Rhodanese like	Phosphatase, Rhodanese like
Hsl1p	1426	1518	43	Yes	Protein kinase	Protein kinase
Hsl7p	788	827	45	Yes	Methyltransferase domain	Methyltransferase domain
Cdc3p	507	520	58	Yes	GTP binding protein	GTP binding protein
Cdc10p	328	322	75	Yes	GTP binding protein	GTP binding protein
Cdc11Ap[b]	411	415	74	Yes	GTP binding protein	GTP binding protein
Cdc11Bp[b]	408		74	Yes	GTP binding protein	
Cdc12p	390	407	78	Yes	GTP binding protein	GTP binding protein
Sep7p	580	551	60	Yes	GTP binding protein	GTP binding protein

[a] Domains identified using InterPro from the UniProtKB/Swiss-Prot database.

[b] Cdc11 duplication first identified by Sophie Brachat in *A. gossypii* genome annotation.

into discontinuous rings at the cortex at the tips of hyphae, along the main hyphae between tips and branches and at branch sites. Rings were composed of discrete "bars" or filaments that were long and faint when present at the tip and short and bright when at the bases of branches or along the main hypha away from the tip (Figure 2A). The rings at the base of branches often appeared asymmetric with the apical half of the ring composed of short, bright bars and the basal half made up of fainter less well-organized bars (Figure 2A, inset). Overall, 18% of septin rings were found at tips, 50% were found at bases of branches, and 32% on the main hyphae (n = 127 septin rings). Fifty percent of the septin rings found on the main hypha were located just beside the spot where a branch emerged. On the basis of this localization of septins and the mitotic index near branches, we would predict that there is a higher proportion of mitotic nuclei in the vicinity of septin rings. In young cells in which septins and tubulin have been visualized by immunofluorescence, 71% of nuclei with mitotic spindles were adjacent to either a tip, main hyphal or branch septin ring and 52% of nuclei with duplicated SPBs were adjacent to septin rings (n = 230 nuclei, Figure 2B). Further support of this observation can be seen in Supplementary Movie 2, in which H4-GFP and SEP7-GFP are both monitored in living cells and mitoses are observed near septin rings.

If septins are required for this spatial pattern of mitotic progression, then cells lacking septins would be predicted to have a random spatial distribution of mitoses and potentially an altered frequency of mitoses. Cells with any one septin (Ag*CDC3*, Ag*CDC10*, or Ag*CDC12*) deleted were viable but had no visible, organized septin rings, presumably due to the higher-order heteromeric septin complex being disturbed due to the loss of any one of the subunits (Figure 2C, septin deletion phenotypes will be described in detail elsewhere). In mutant cells lacking the septin AgCdc12p both mitotic nuclei and nuclei with duplicated SPBs were no longer commonly observed at branchpoints as seen in wt cells and instead appeared to be randomly distributed in hyphae. In wt cells grown in liquid, 45% of nuclei were near a branch, whereas in Ag*cdc12*Δ only 13% were at branches (N >200 nuclei). In contrast, similar proportions of dividing nuclei in Ag*cdc12*Δ mutants (32%) were observed in growing tip regions compared with wild type (30%), suggesting that the septin ring at branchpoints wields greater influence over the nuclear cycle than the diffuse structures at the tips of hyphae. Thus at least certain septin rings seem to provide spatial directions to the mitotic machinery and potentially help to establish a subcellular region that favors nuclear progression.

How might the septins locally promote mitosis? Given their role as scaffolds for a multitude of factors at the mother-bud neck in budding yeast, it is conceivable that the septins are similarly recruiting either mitosis-promoting or -inhibiting factors to branching spots in *A. gossypii* cells. In budding yeast, the proteins involved in the morphogenesis checkpoint are recruited to septins for the inhibition of the CDK inhibitor Swe1p. We identified the *A. gossypii* homologues of the key components of the *S. cerevisiae* morphogenesis checkpoint as a basis to begin evaluating if these factors may be used to direct where mitosis is taking place in multinucleated cells that do not bud. Homology and length of these factors vary tremendously; however, core domains are conserved and they are present in syntenic positions of the genome, suggesting that protein functions such as kinase (AgSwe1p) and phosphatase (AgMih1p) activity are conserved (Table 4).

AgHsl7p Localizes to Septin-dependent Cortical Rings

To begin to evaluate if the septins concentrate CDK regulators near branchpoints, we attempted to localize some of the *A. gossypii* homologues of the budding yeast morphogenesis checkpoint proteins. AgSwe1p was not visible when tagged either with GFP or epitopes in normally growing cells but AgHsl7p, a possible AgSwe1p regulator, was visible in *A. gossypii* cells. AgHsl7p-GFP expressed from the endogenous promoter was concentrated in discontinuous rings reminiscent of septin rings (Figure 3, A–D). Colocalization by immunostaining against GFP and Cdc11p showed that in fact AgHsl7p-GFP colocalized with some but not all septin rings, and in no case was AgHsl7p-GFP observed in the absence of a septin ring (unpublished data). These results could be due to AgHsl7p associating preferentially with certain types of septin ring organizations or AgHsl7p interacting only transiently with organized septins. AgHsl7p-GFP was not observed in cortical rings in either Ag*cdc12*Δ or Ag*hsl1*Δ mutant cells, suggesting that this likely AgSwe1p regulator is concentrated in specific regions of the cell by septins (Figure 3, E and F).

AgSwe1p Regulation Influences the Position of Mitoses

To evaluate if AgSwe1p, its possible regulators (AgHsl1p, septins), or the opposing phosphatase, AgMih1p, contribute to

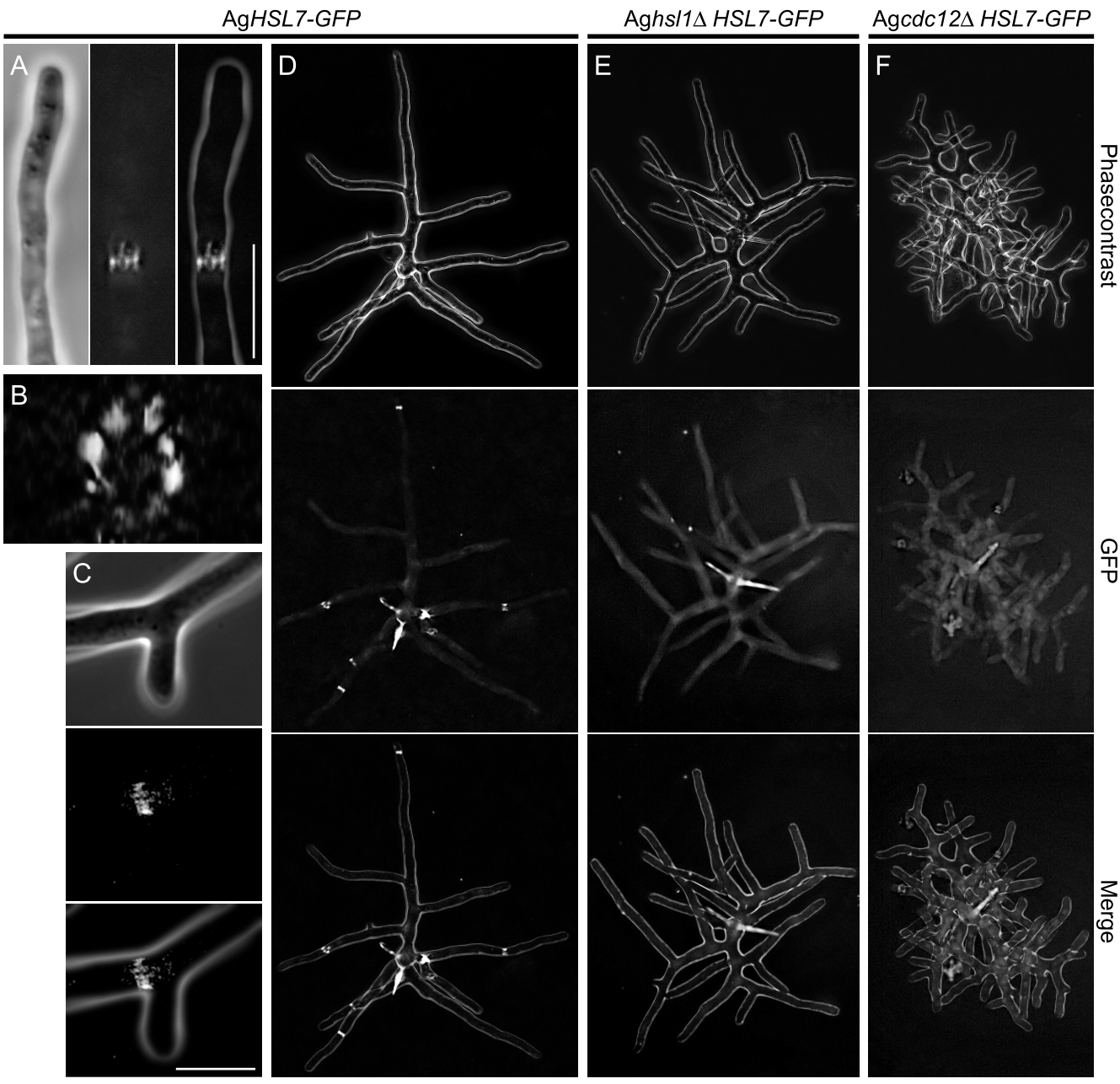

Figure 3. AgHsl7p localizes to septin-dependent cortical rings. (A–D) Ag*HSL7-GFP* (ASG41) cells were grown for 12 h at 30°C and then imaged live. (B) 90° 3D reconstruction of the discontinuous ring shown in A. (E and F) Ag*cdc12*Δ*HSL7-GFP* (AgHPH19) and Ag*hsl1*Δ*HSL7-GFP* (AgHPH20) were grown for 12 h at 30°C and then imaged live. Phase contrast, fluorescence and merged images are ordered from left to right (A) or from top to bottom (C–F). Bars, 10 μm.

either the spatial pattern or the kinetics of nuclear division, single and combination mutants were generated and evaluated for growth, nuclear density, nuclear division cycle stage, and position of mitoses. Under normal growth conditions in rich media all mutant cells, with the exception of septin mutants, grew with rates comparable to wild type (Figure 4A). Septin mutants had reduced growth rates (70% of wild type) and aberrant morphology with wide, kinked hyphae. Nuclear density was comparable to wild type (4.6 μm between nuclei) in Ag*hsl1*Δ (3.8 μm), Ag*swe1*Δ (3.8 μm), Ag*mih1*Δ (3.8 μm), and Ag*cdc12*Δ (4.7 μm) mutants (N >300 nuclei scored for each strain, Figure 4A). The nuclear division cycle phase proportions were similar to wild type for the different mutant strains (nuclear cycle stage scoring based on spindle appearance by anti-tubulin immunofluorescence, Figure 4B); however, there was a moderate increase in the percentage of metaphase and anaphase nuclei in Ag*hsl1*Δ (12% vs. 7% in wt) and Ag*cdc12*Δ (14%) mutants, suggesting there may be some delay late in the nuclear division cycle due to the absence of these proteins. Based on homologues in other systems, Ag*hsl1*Δ*mih1*Δ or Ag*cdc12*Δ*mih1*Δ double mutants would be predicted to have a synthetic interaction because of the release of inhibition of AgSwe1p in the absence of the phosphatase, AgMih1p, that likely opposes AgSwe1p. In *S. cerevisiae* the analogous mutations lead to inviable cells. There is no additive effect in terms of growth, nuclear density, or nuclear division cycle stage;

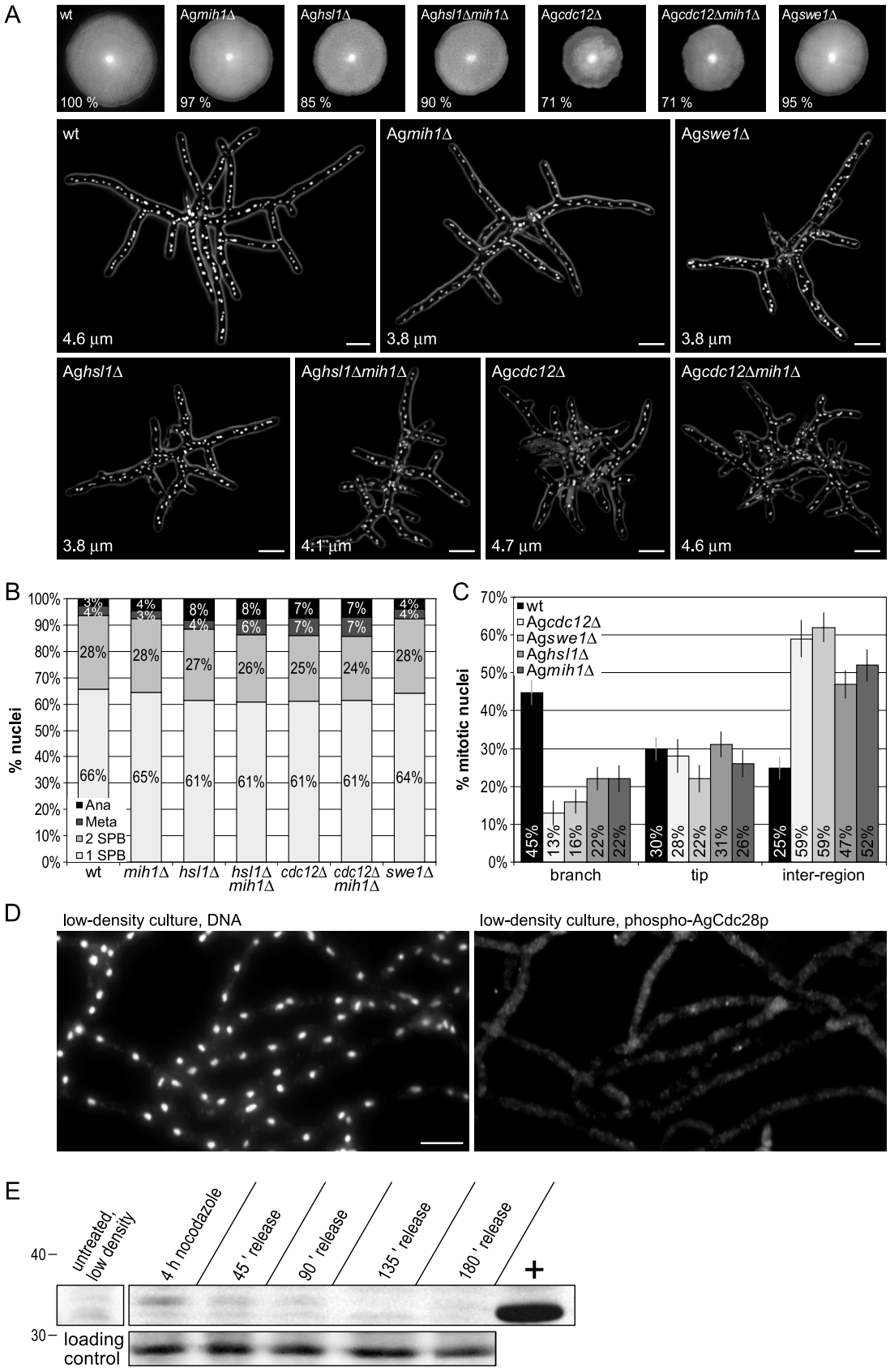

Figure 4. AgSwe1p regulation influences the position of mitoses. (A) Radial growth on solid medium of wild type (*leu2*Δ *thr4*Δ) and deletion mutants Ag*mih1*Δ (AgHPH23), Ag*hsl1*Δ (hsl*1*ΔNAT1), Ag*hsl1*Δ*mih1*Δ (AgHPH28), Ag*cdc12*Δ (AgHPH15), Ag*cdc12*Δ*mih1*Δ (AgHPH27), and Ag*swe1*Δ (ASG35) compared with wild type (100%; top). A small piece of homokaryotic mycelium (~1 mm^3) from each strain was spotted

however, in these double mutant cells in *A. gossypii* (Figure 4, A and B). These data combined suggest that despite the conservation of this network in the genome there is a minimal "global" role for the septins/Hsl1p/Swe1p, and Mih1p in *A. gossypii* for regulating the frequency of nuclear division under standard laboratory (low-density/rich-nutrient) growth conditions.

The septins clearly influence the position of mitosis so to further address if this functions through local AgSwe1p regulation as may be predicted based on the AgHsl7p localization, the position of mitotic nuclei relative to branchpoints and to tips were scored in Ags*we1*Δ, Ag*hsl1*Δ, and Ag*mih1*Δ cells. Mitotic nuclei in each of these mutant cells were similarly distributed as in septin mutants such that they were found more frequently in the interregion of hyphae than at branch sites, compared with wild type (Figure 4C). The frequency of tip region mitoses, however, was not significantly altered in any of the mutant cells. Thus in both cells lacking AgSwe1p or with potentially misregulated AgSwe1p, the mitosis-promoting zone of branchpoints seems to be disturbed. Thus septins may normally function to locally relieve AgSwe1p-based nuclear cycle inhibition at branching points.

To determine if AgSwe1p spatially influences mitosis by phosphorylating the tyrosine 18 residue of the CDK (the analogous tyrosine that has been shown in a variety of systems to be a substrate of Swe1/wee1 kinases), we applied a phospho-specific anti-cdc2(Tyr15) antibody to cells and cell extracts. First, phosphorylated CDK (AgCdc28p) was assayed for in cells by immunofluorescence to see if a subset of nuclei, such as those in the interregion far from branchpoints, may be enriched for modified AgCdc28p (Figure 4D). No phosphorylated protein was detected by this method, but potentially this could be due to technical problems resolving the protein with this antibody by immunofluorescence. Thus, whole cell extracts were also generated to evaluate if the antibody can recognize the *A. gossypii* CDK by Western blot. Minimal phosphorylation on AgCdc28p, however, was apparent in either asynchronously growing cells or cells that had been artificially synchronized (~70% synchrony) in G2/M with nocodazole and released for progression through mitosis (Figure 4E). Thus, although AgSwe1p and septins both seem to contribute to the spatial control of mitosis, it is still unclear if they function through tyrosine phosphorylation of the CDK.

Figure 4 (cont). on full medium plates and grown for 4 d. Nuclei visualized in different strains (bottom). Cells (same strains as above) were grown overnight at 30°C in selective conditions and fixed and processed for Hoechst dye staining. Numbers indicate average distance between two nuclei. (B) Percentage of nuclei in different nuclear division cycle stages evaluated by Hoechst and anti-tubulin staining (Ana: anaphase; Meta: metaphase; 2 SPB: 2 spindle pole bodies; 1 SPB: 1 spindle pole body). (C) Percentage of mitoses found at sites of branch formation, at tips and in the interregion of hyphae evaluated by Hoechst and anti-tubulin staining. Bars, SE. (D) Wild-type cells (*leu2*Δ *thr4*Δ) grown under low-density conditions were stained with Hoechst for DNA visualization (left) and assayed for phosphorylated CDK by immunofluorescence using the anti-phospho-cdc2(Tyr15) antibody (right). (E) Protein extracts from wt cells (*leu2*Δ *thr4*Δ) grown under low-density conditions and then arrested and released from nocodazole were assayed for phosphorylated CDK on a Western blot, using the anti-phospho-cdc2(Tyr15) antibody. A nonspecific band from the Ponceau red treated membrane was used as loading control. Extracts from the *S. cerevisiae* strain DLY5544 (*cdc12-6, PGAL1-SWE1*) served as positive (+) control for this and all following Western blots. The numbers indicate the molecular weight in kDa. Bars, 10 μm.

AgCdc28 Is Phosphorylated on Tyrosine 18 when Cells Are Starved for Nutrients

The absence of detectable CDK tyrosine phosphorylation led us to ask if we could ever observe such modifications during the *A. gossypii* nuclear division cycle, perhaps only under certain environmental conditions. Given the common role of Wee1 kinases in different checkpoint responses across eukaryotes, we evaluated if AgCdc28p was phosphorylated when cells were exposed to potential checkpoint triggers and environmental stresses including hydroxyurea (to impair DNA replication), nocodazole (to impede spindle assembly), starvation, osmotic shock, and high temperature (42°C). No or limited phosphorylation was detected using the anti-phospho-cdc2(Tyr15) antibody on whole cell extracts from cultures treated with hydroxyurea or nocodazole (Figure 5A). High-temperature stress and osmotic shock resulted in moderate phosphorylation on a protein of the predicted size of AgCdc28p. Surprisingly, starvation that was induced by high-density growth (evaluation described in *Materials and Methods*) resulted in a level of phosphorylation that was markedly stronger than in any other condition tested (Figure 5A).

This phosphorylated form of AgCdc28p was visible both in whole cell extracts from high-density cultures and in the nuclei of intact cells visualized by immunofluorescence (Figure 5B). The high-density/nutrient deprivation–induced phosphorylation was reversed, along with the phenotype associated with starvation (prominent vacuoles) but relatively slowly upon feeding the cells with fresh media (Figure 5C). The phosphorylation was reduced after 3 h in fresh media and at the minimal levels found in low-density cultures after 5 h.

To confirm that the phosphorylation observed is as predicted on the tyrosine 18 residue of AgCdc28p, this residue was mutated to phenylalanine, which should be nonphosphorylatable. The phosphorylated AgCdc28p recognized in wt, high-density cultures is not present in lysates generated from Ag*cdc28*Y18F cells grown to similar high density (Figure 5D). This indicates that the anti-phospho-cdc2(Tyr15) antibody is recognizing the conserved tyrosine phosphorylation on the *A. gossypii* CDK.

This phosphorylated AgCdc28p observed in densely grown cultures could be formed in response to nutrient deprivation or could be a density-dependent reaction to a quorum-sensing molecule that accumulates at high density. Several approaches were taken to attempt to distinguish between these possibilities. First, cells were treated with rapamycin which likely inhibits the kinase AgTor1/2p, which has a conserved role in nutrient sensing in a variety of eukaryotes. Inhibition of Tor kinase mimics starvation in many cells and in budding yeast simulates nitrogen starvation (Martin and Hall, 2005). AgCdc28Y18 phosphorylation clearly accumulated with time in the presence of rapamycin even in cells grown at low density in rich-nutrient conditions (Figure 6A). Thus, the appearance of the phosphorylated form did not depend on high density here but did appear during this mock starvation. Furthermore, when cells grown at low density are transferred to MOPS/KCl buffer (osmotically stable but without nutrients) to induce rapid low-density starvation, CDK phosphorylation appeared within 30 min and accumulated to levels comparable to high-density starvation by 105 min (Figure 6A). Finally, the response was independent of the type of nutrient that was restricted and was observed when either carbon (AFM with 0.1% glucose) or nitrogen (ASD-Asn or with one quarter amino acid con-

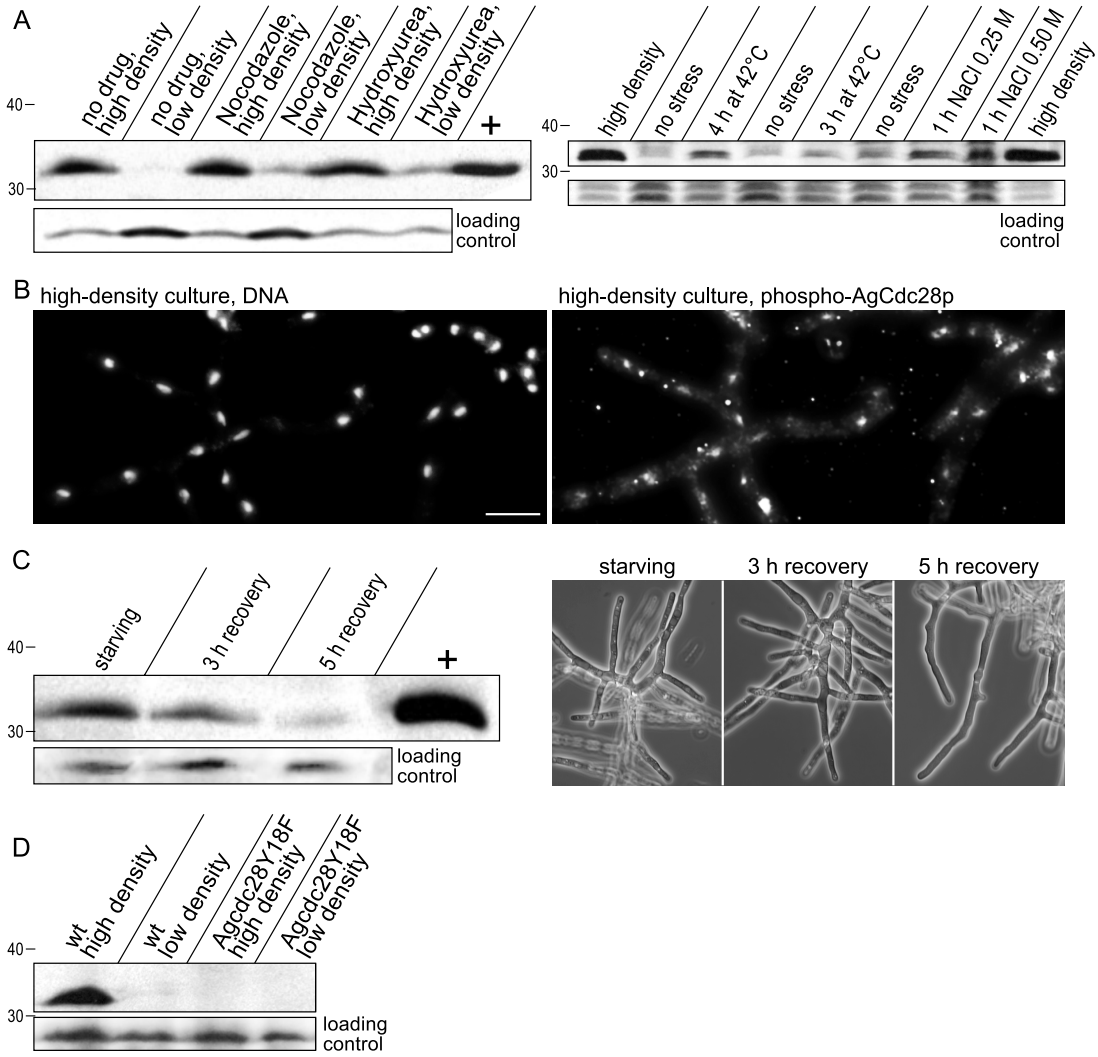

Figure 5. AgCdc28 is phosphorylated on tyrosine 18 when cells are starved for nutrients. (A) Wild-type cells (*leu2*Δ *thr4*Δ) were grown for 12 h at 30°C before exposure to checkpoint stimuli or environmental stresses followed by lysis and Western blotting of whole cell extracts using the anti-phospho-cdc2(Tyr15) antibody. When not indicated otherwise, the cells were grown at low density before applying the various stresses. Nocodazole was used at 15 μg/ml and hydroxyurea at 50 mM. As loading control, a nonspecific cross-reacting band was used for the blot at the left, and a nonspecific band from the Ponceau red treated membrane was used for the blot at the right. (B) Wild-type cells (*leu2*Δ *thr4*Δ) grown under high-density conditions for 16 h were stained with Hoechst for DNA visualization (left) and assayed for phosphorylated CDK by immunofluorescence using the anti-phospho-cdc2(Tyr15) antibody (right). Bar, 10 μm. (C) Wild-type cells (*leu2*Δ *thr4*Δ) were grown under high-density conditions in 20 ml of AFM until prominent vacuole formation was observed (18 h). The cells were washed and resuspended in 200 ml of fresh AFM to recover. Samples were taken after 3 and 5 h, cells were lysed, and the levels of CDK phosphorylation in whole cell extracts were detected by Western blotting using the anti-phospho-cdc2(Tyr15) antibody (left). A nonspecific cross-reacting band was used as loading control. The degree of vacuolization was observed by phase-contrast microscopy (right). (D) Wild-type (*leu2*Δ *thr4*Δ) and Ag*cdc28*Y18F (AgHPH36) cells were grown to the indicated densities, lysed, and processed by Western blot using the anti-phospho-cdc2(Tyr15) antibody. A nonspecific cross-reacting band was used as loading control.

centration) was the limiting resource even when cells were grown to low density (Figure 6B). Thus, AgCdc28Y18 phosphorylation appears in response to nutrient deprivation rather than other possible signals that may accumulate at high-density growth.

The Nuclear Cycle Is Delayed in Specific Stages of Division during Starvation

If phosphorylation of the CDK is inhibitory, as would be predicted, then we would expect a delay or inhibition of the nuclear cycle that leads to a change in nuclear density when cells are limited for nutrients. In fact the distance between nuclei was significantly different between high- and low-density–grown cultures. Nuclei from cells grown to low density, which presumably were not yet limited for nutrients, were an average of 4.6 μm apart, whereas in nutrient-limited conditions this distance expanded to 10.2 μm (N >500 nuclei). Ag*cdc28*Y18F cells, which are resistant to CDK phosphorylation, showed an intermediate nuclear density in low nutrients of 7.9 μm (N >300 nuclei), suggesting that some but not all of the delay in nuclear division is due to tyrosine phosphorylation–based inhibition of AgCdc28p. Furthermore, it is clear that polarized hyphal growth continues (presumably until internal energy supplies such as lipid droplets are depleted), whereas the nuclear cycle is delayed or blocked under starvation.

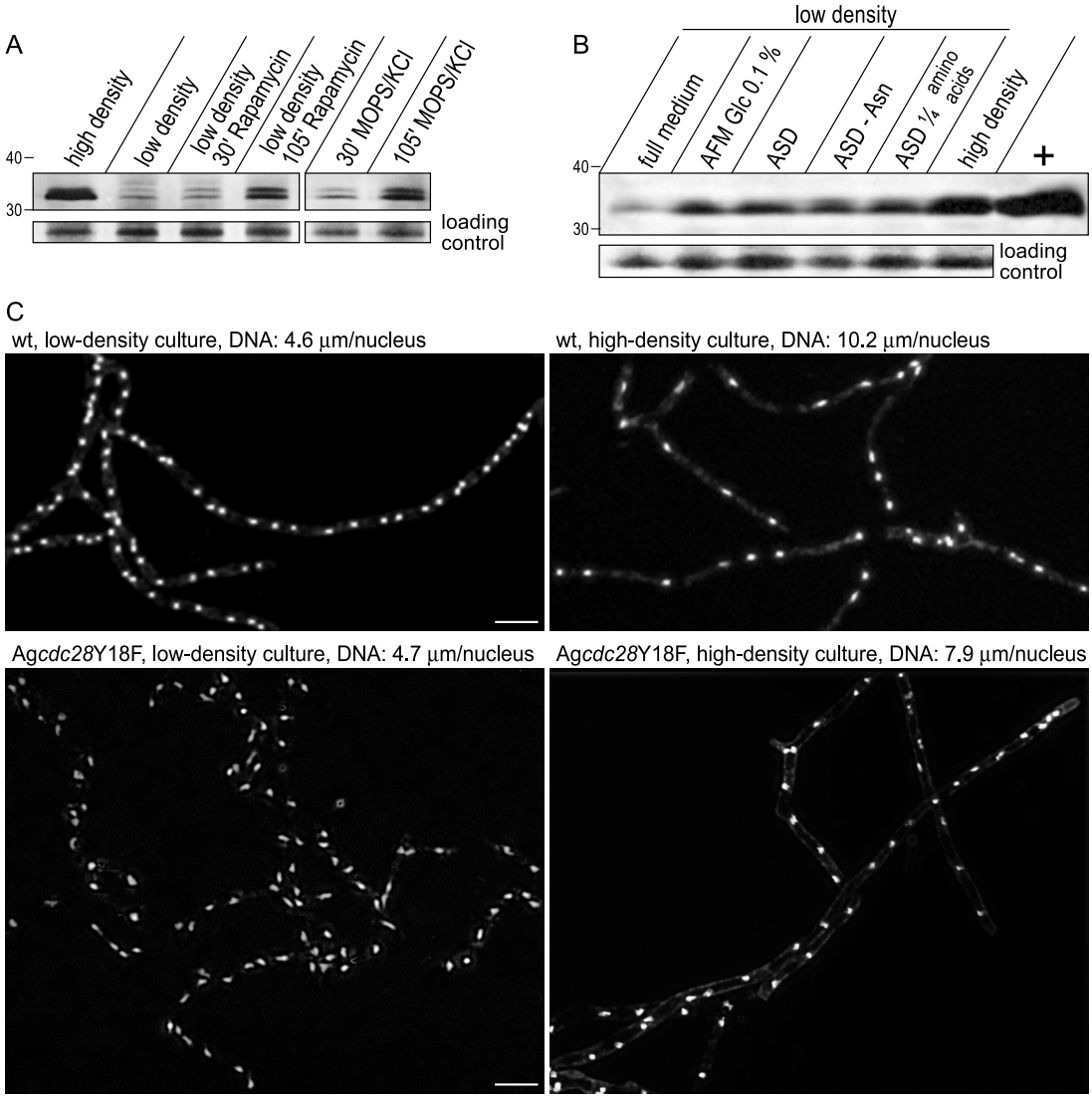

Figure 6. CDK phosphorylation produces nuclear delay in nutrient deprivation. (A) Wild-type cells (*leu2*Δ *thr4*Δ) were grown under low-density conditions before adding 200 nM rapamycin or transferring the cells to MOPS/KCl (40 mM MOPS, pH 7.0, 137 mM KCl) except for the left lane where cells were grown to high density for a positive control. CDK phosphorylation was detected by Western blotting as described above. (B) Low-density wt cells (*leu2*Δ *thr4*Δ) were grown in full medium (AFM) for 12 h before shifting them into media limited for different resources: AFM Glc 0.1% (20 times less glucose than standard growth media), ASD (synthetic media without yeast extract), ASD-Asn (synthetic media lacking asparagine), and ASD with 0.25 normal amino acid concentration. Samples were taken 5 h after the media shift and assayed for CDK phosphorylation as described above. (C) Wild-type (*leu2*Δ *thr4*Δ) and Ag*cdc28*Y18F (AgHPH36) cells were grown to the noted densities, fixed, and stained with Hoechst to visualize nuclei. Bars, 10 μm.

If such a delay is stochastic such that limited nutrients can block nuclei in any stage of the nuclear division cycle, then high-density cultures would be expected to have similar proportions of nuclei in each nuclear division cycle stage as those found in low-density cultures. If, however, the delay is regulated such that it occurs in a specific window of time, the proportions of nuclei in each nuclear division cycle stage should vary between the different growth conditions. Under high-density growth conditions, more nuclei accumulated in cells with duplicated SPBs and metaphase spindles compared with low-density cultures. Cells in high-density cultures contained 41% nuclei with duplicated SPBs compared with 28% in low density and 16% metaphase nuclei compared with 4% in low-density cultures (N >200 nuclei). Thus the deprivation of nutrients leads to accumulation of nuclei in specific stages of division, both just before and during metaphase (summarized as part of Figure 7B).

AgSwe1p Is Responsible for AgCdc28Y18 Phosphorylation and Mitotic Inhibition in Starving Cells

Phosphorylation on Tyr18 of AgCdc28p mediates a delay or arrest in the nuclear cycle in response to nutrient limitation. Is AgSwe1p responsible for this inhibition of AgCdc28p? As in Agcdc28Y18F mutants, *Agswe1*Δ mutants also failed to accumulate phosphorylated AgCdc28p in high-density conditions in contrast to wt cells (Figure 7A). Surprisingly, Ag*mih1*Δ mutants had comparable levels of phosphorylation to wt cells, suggesting that under these conditions AgMih1p may normally be down-regulated. Additionally, low-density grown Ag*swe1*Δ cells that had been incubated

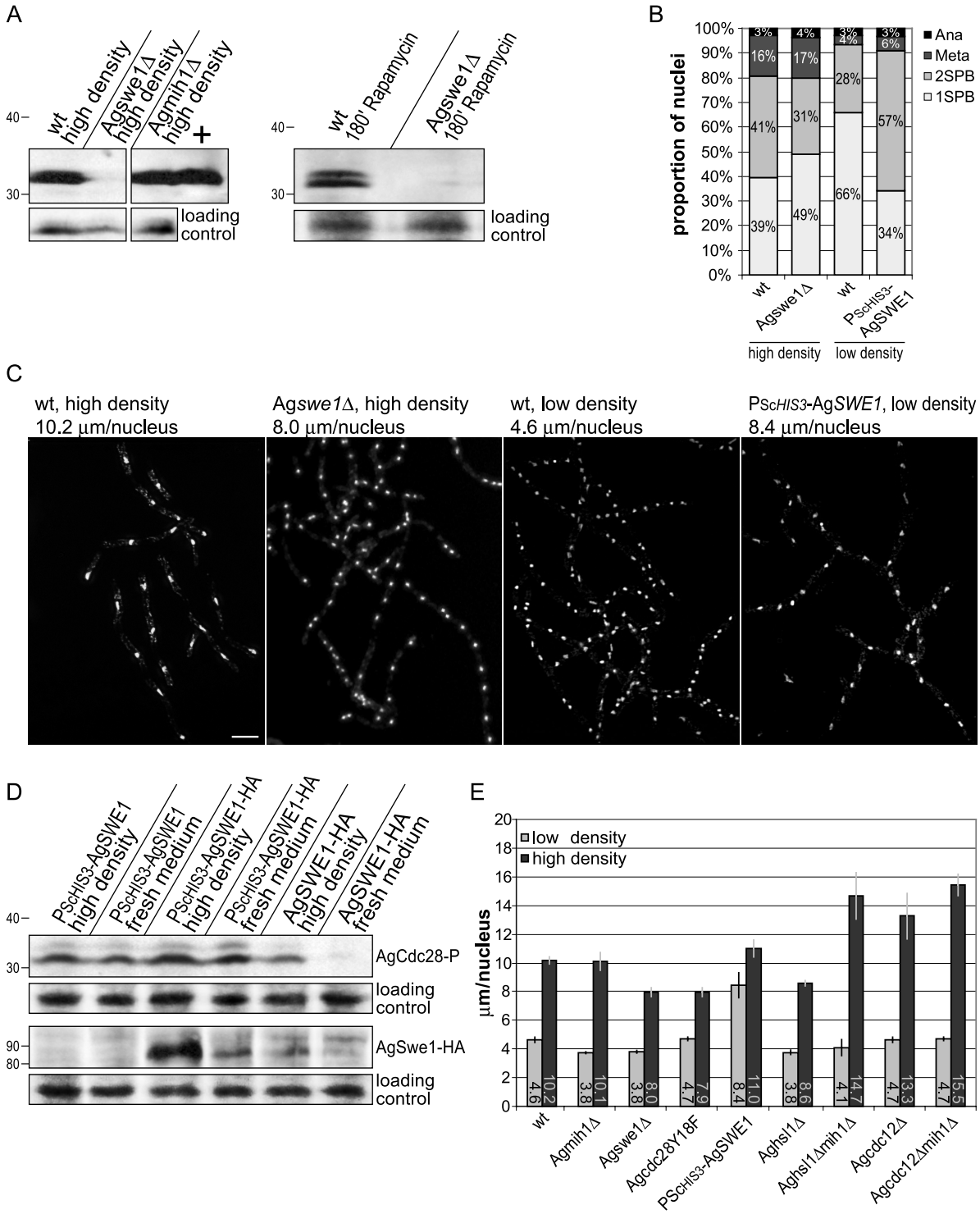

Figure 7. AgSwe1p is the kinase responsible for AgCdc28Y18 phosphorylation. (A) Wild-type (*leu2*Δ *thr4*Δ), Ag*swe1*Δ (AgHPH24), and Ag*mih1*Δ (AgHPH23) cells were grown to high density, and whole cell extracts were assayed for CDK phosphorylation as described above (left). Wild-type (*leu2*Δ *thr4*Δ) and Ag*swe1*Δ (AgHPH24) cells were grown overnight to low density and then incubated with rapamycin (200 nM). A nonspecific cross-reacting band was used as loading control. (B) Wild-type (*leu2*Δ *thr4*Δ), Ag*swe1*Δ (AgHPH24), and PSc*HIS3*-Ag*SWE1* (AgHPH37) cells were grown at 30°C to high/low density and then fixed and processed for anti-tubulin immunofluorescence to evaluate the percentage of nuclei in different nuclear division cycle stages. (C) Nuclei of cells grown for (B) visualized by Hoechst staining. Bar, 10 μm. (D) Whole cell extracts from PSc*HIS3*-Ag*SWE1* (AgHPH37, lanes 1 and 2), PSc*HIS3*-Ag*SWE1-6HA* (AgHPH38, lanes 3 and 4), and Ag*SWE1-6HA* (AgHPH39, lanes 5 and 6) were generated from cells grown to either high or low density. Extracts were then probed by Western blot using either the anti-phospho-cdc2(Tyr15) or anti-HA antibody. A nonspecific cross-reacting band was used as loading control. (E) Wild-type (*leu2*Δ *thr4*Δ), Ag*mih1*Δ (AgHPH23), Ag*swe1*Δ (AgHPH24), Ag*cdc28Y18F* (AgHPH36), PSc*HIS3*-Ag*SWE1* (AgHPH37), Ag*hsl1*Δ (hsl1ΔNAT1), Ag*hsl1*Δ*mih1*Δ (AgHPH28), Ag*cdc12*Δ (AgHPH15), and Ag*cdc12*Δ*mih1*Δ (AgHPH27) cells were grown to either high or low density and fixed, and nuclei were visualized by Hoechst staining to calculate the average distance between two nuclei for each strain and condition. Error bars reflect weighted SEs.

with rapamycin also did not have detectable AgCdc28p phosphorylation, showing that the rapamycin induced modification is also executed by AgSwe1p (Figure 7A).

Are the altered nuclear density and nuclear division cycle proportions observed under high-density conditions due to the action of AgSwe1p? Ag*swe1*Δ cells grown to high density failed to respond as strongly to these conditions, but still showed some increase in nuclear density (8.0 μm [N >500 nuclei] compared with 7.9 μm in Ag*cdc28*Y18F and more than 10 μm in wild type, Figure 7C). *Agswe1*Δ mutant cells had fewer nuclei with duplicated SPBs than wt cells at high density but retained a similar proportion mitotic nuclei (Figure 7B). These results suggest that AgSwe1p induced AgCdc28Y18 phosphorylation is responsible for a delay in nuclear division in G2 and that some other factors are responsible for the altered proportion of metaphase nuclei in high-density growth.

To determine if AgSwe1p activity was sufficient for AgCdc28p phosphorylation and altered nuclear division even in the absence of high-density starvation, AgSwe1p was overexpressed in cells grown in low-density conditions. For this experiment the AgSwe1p promoter was replaced with the *S. cerevisiae HIS3* promoter, which leads to high, constitutive expression of proteins in *A. gossypii* (Dominic Hœpfner, personal communication). Protein levels were assayed by Western blot against a 6HA-epitope tag fused to the C-terminus of AgSwe1p to confirm that the *HIS3* promoter leads to overexpression of the AgSwe1p protein (Figure 7D). Additionally, Ag*SWE1* expression under its own promoter was evaluated for regulation and to confirm that the HA fusion protein was functional during high- and low-density growth. Under control of the native promoter, AgSwe1p-6HA was barely detected in low density cultures, whereas in high-density growth, it was somewhat more abundant. Unlike in wt cells, phosphorylated AgCdc28p was readily detected in low-density conditions when AgSwe1p was overexpressed from the *ScHIS3* promoter (lanes 2 and 4 compared with lane 6, Figure 7D).

To determine if this Y18 phosphorylation of AgCdc28p could alter nuclear cycle progression even in low-density cultures, nuclear density was evaluated in these cells overexpressing AgSwe1p. The overexpressed AgSwe1p and presumably the subsequent AgCdc28p phosphorylation led to a 50% decrease in nuclear density with an average distance between nuclei of 8.4 μm compared with 4.6 μm wild type at low density (Figure 7C). Additionally, the overexpressed AgSwe1p led to a dramatic delay in the nuclear division cycle leading to a population in which almost 60% of nuclei had duplicated SPBs compared with only 28% in wt, low-density cultures, further suggesting that AgSwe1p-induced AgCdc28p phosphorylation acts before metaphase (Figure 7B).

Nuclear Delay in Response to Starvation Is Exacerbated in Septin Mutants

Is AgSwe1p-induced AgCdc28p phosphorylation in response to low nutrients regulated by septins and AgHsl1p? If these factors do negatively regulate AgSwe1p in high-density growth, then cells lacking these controls may show an exacerbated response to starvation with even larger distances between nuclei. To begin to evaluate if these factors contribute to AgSwe1p regulation during starvation, nuclear density was evaluated in Ag*hsl1*Δ, Ag*cdc12*Δ, Ag*hsl1*Δ, Ag*mih1*Δ, and Ag*cdc12*Δ*mih1*Δ mutants in high-density cultures. Ag*cdc12*Δ (13.3 μm), Ag*hsl1*Δ*mih1*Δ (14.7 μm), and Ag*cdc12*Δ*mih1*Δ (15.5 μm) mutants all had in average higher nuclear densities than wild type (10.2 μm) or even cells overexpressing AgSwe1p (11.0 μm). One caveat to these experiments however is that the slower growth rate of septin mutants necessitates a longer period of overall growth to achieve high density, and thus the growth time is not identical between septin mutant strains and other strains. Nonetheless these data raise the possibility that the septins and AgHsl1p contribute some form of negative regulation to AgSwe1p during high-density growth (Figure 7E).

DISCUSSION

In this work, we have sought to identify mechanisms for how mitosis may be spatially regulated in multinucleated hyphal cells. We have shown that septins promote mitosis in the vicinity of branchpoints and that this is likely regulated through AgSwe1p activity. This represents a novel role for a Wee1 kinase in spatially directing mitosis in multinucleated cells. AgSwe1p also promotes AgCdc28Y18 phosphorylation to limit mitosis when these cells are starved for nutrients. Based on this data, it appears that Swe1p in *A. gossypii* responds both to intrinsic morphogenesis cues and external environmental conditions. Here we discuss these data and propose a hypothetical model in which activity of AgSwe1p and assembly of septins may enable these multinucleated cells to react to a spatially limited pool of nutrients and restrict mitoses to the area of the nutrient source (Figure 8).

How are the septins locally influencing mitosis in uniform, rich-nutrient growth conditions? Septin proteins have different appearing organizations depending on their location in hyphae and potentially these morphologically different structures are also functionally distinct. Rings composed of elongated bands form at the tips and more compact rings of short septin bars appear more distant from the growing tip along the main hyphae, and asymmetric bar structures are featured at most branchpoints. Conceivably, these different varieties of septin rings could recruit different pools of proteins, attract the same proteins with different affinities, or function to delineate different plasma or organelle membrane domains. Additionally, it is still unclear if all the different septin proteins are uniformly recruited to each type of ring organization. Support for functional difference in the structures comes from the observation that only mitosis frequency near branches, not at tips, is diminished in septin mutants, which are missing all visible, organized septin rings. Thus, the asymmetric structure that decorates the bases of branches and potentially the rings of the main hyphae near branches, seems to be pivotal in directing mitoses in this area. Notably, this influence over the nuclear division cycle is transient and is most pronounced as the branch tip emerges, as seen in Supplementary Movie 1. As the branch matures, although the ring persists, there are fewer mitoses in this area, suggesting a decay of the local mitotic inducing potential with time. This coincides with subtle changes in the structure of the asymmetric ring (greater distance between the two halves of the ring; see inset of Figure 2A); however, it is unclear if this change is relevant for mitosis regulation.

Complex patterns of septin organization have also been observed in a variety of other multinucleated and filamentous fungi (Douglas *et al.*, 2005; Gladfelter, 2006). In *Candida albicans* hyphae, the septins establish a nuclear division plane in hyphal cells. In *Aspergillus nidulans*, septin ring assembly at the bases of branches coincides with the reentry of nuclei into mitosis, but the link between septins and the nuclear division machinery is still unknown in this system (Westfall and Momany, 2002).

What are possible ways the septin rings at branchpoints could influence the mitotic machinery in *A. gossypii*? Based

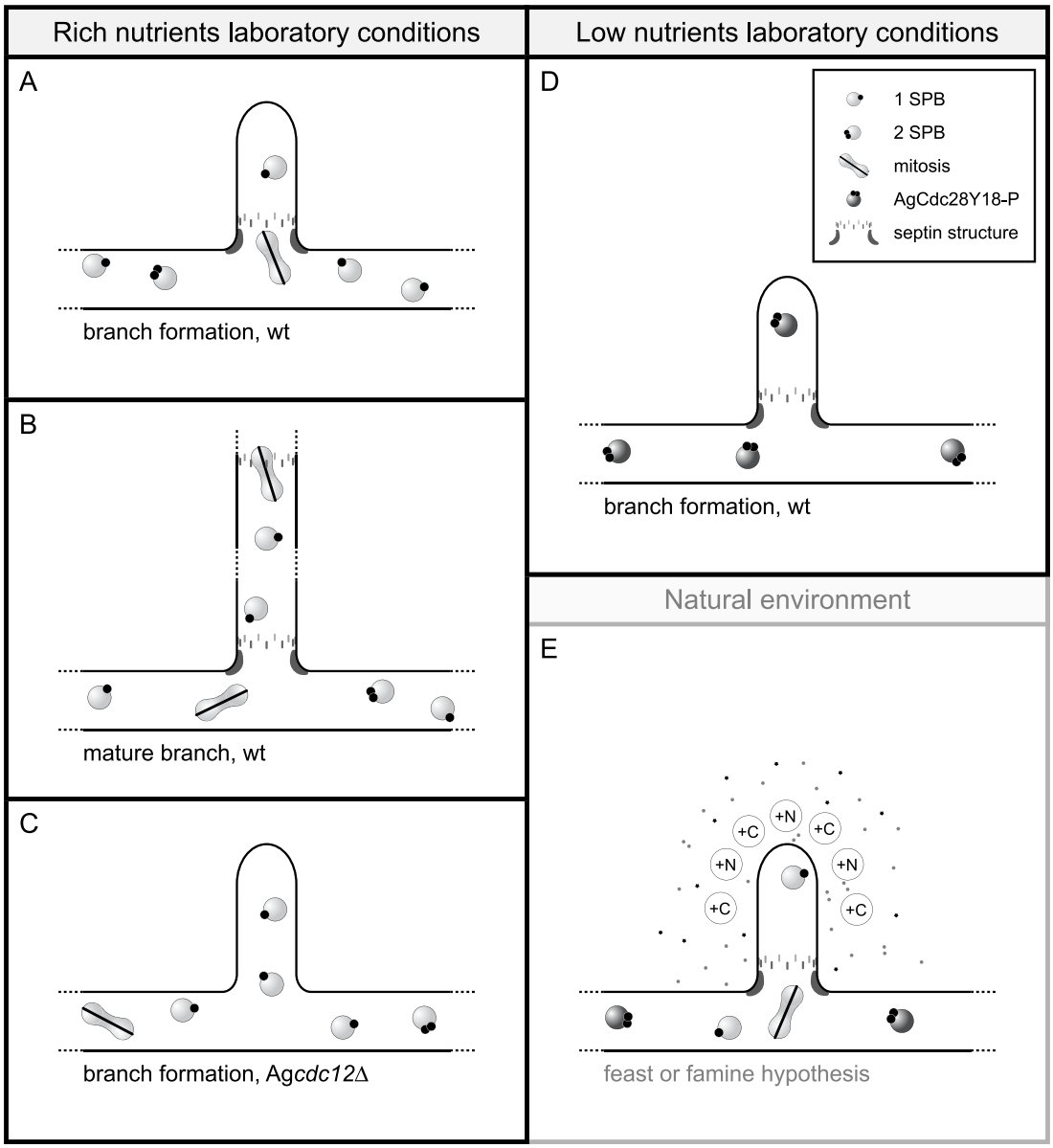

Figure 8. Model of spatial control of mitosis by septins and nutrient availability. (A) Wild-type cells grown in the laboratory have mitoses enriched at branch sites near assembled septin rings. (B) As branch sites mature, new septin rings in developing branches acquire mitosis promoting capacity, leading to mitotic events in interregions. (C) Mitoses are no longer localized preferentially to branch sites in cells lacking septins. (D) In low-nutrient conditions, nuclei are arrested or delayed with duplicated SPBs and high CDK-Tyr 18 phosphorylation levels. (E). Hypothesis for how mitoses may be spatially controlled in response to heterogeneous nutrient supplies in the natural world, where a single hypha may simultaneously experience "feast and famine" conditions. Local pools of nutrients may trigger assembly of a septin ring, which in turn promotes local mitosis through the down-regulation of AgSwe1p, enabling the cell to exploit nutrients without duplicating nuclei distant to nutrient source.

on the wiring of the morphogenesis checkpoint in *S. cerevisiae* and conservation of these factors, it is easy to hypothesize that septins direct mitosis through the recruitment and local inactivation of AgSwe1p. Potentially in unbranched areas of cells, some nuclei are delayed in division by active AgSwe1p. This delay then is relieved upon septin ring formation at branchpoints, which leads to a local depletion/inhibition of AgSwe1p and then nuclear division at such sites. The observation that deletion of Ag*SWE1*, Ag*HSL1*, Ag*MIH1*, or Ag*CDC12* similarly shifts mitoses away from branches to random positions supports the possibility that the balance of AgSwe1p activity controls the spatial pattern of mitosis. Cells lacking AgSwe1p would no longer have the means to limit mitoses in unbranched areas, and cells lacking septins would not be able to promote mitoses at branches, both of which result in random division phenotypes. Furthermore, the localization of AgHsl7p, whose homologue functions in *S. cerevisiae* as an adaptor that helps bring Swe1p to the septins where it is targeted for degradation, is suggestive that the links in this regulatory system may be preserved in *A. gossypii*. Thus, in response to some cell intrinsic patterning signals that direct branching in rich nutrient conditions, there is evidence that the septins may direct mitosis spatially through AgSwe1p activity.

There are some problems, however, in overlaying the details of the *S. cerevisiae* morphogenesis checkpoint system onto the *A. gossypii* spatial control system that functions in response to cell intrinsic cues. AgHsl7p is not observed at all branch septin sites and rather seems to be more common at septin rings on the main hyphae, although this could just be due to detection problems. Additionally, the AgHsl7p has a key residue differences in its sequence compared with the ScHsl7p at phenylalanine 242. When Sc*HSL7*F242 is mutated to leucine, the same substitution observed in the *A. gossypii* sequence, ScHsl7p no longer can interact with ScHsl1p, and ScSwe1p is no longer targeted for degradation in budding yeast cells (Cid *et al.*, 2001). This raises the question as to whether AgHsl1p and AgHsl7p form a stable complex that could promote AgSwe1p recruitment. More notably, no AgCdc28Y18 phosphorylation is detectable in cells grown in high nutrient conditions, suggesting that the septins and AgSwe1p could function through other means to regulate the nuclear cycle machinery and influence the spatial balance of mitoses in this condition.

What are alternative modes by which the septins and AgSwe1p may function here? Certainly septins recruit a plethora (>50) of proteins to the mother-bud neck in budding yeast so conceivably the *A. gossypii* septins are recruiting and either inhibiting/activating additional cell cycle factors locally at branches (Gladfelter *et al.*, 2001). Alternatively, the septins may interact more directly with nuclei at branches by capturing the ends of astral microtubules. Such associations have been observed by tubulin immunofluorescence of *A. gossypii* cells (A. Gladfelter, unpublished results) and potentially such physical connections, which may generate tension on the astrals, could be a trigger for mitosis. AgSwe1p may itself have other targets than AgCdc28p that are relevant for nuclear cycle progression, and potentially AgSwe1p-dependent phosphorylation impacts their activity and in turn progression. Or AgSwe1p may be able to directly inhibit AgCdc28p independent of Y18 phosphorylation, and there is actually precedent for this alternative inhibition of the CDK in the morphogenesis checkpoint in budding yeast (McMillan *et al.*, 1999b).

Despite a change in the position of mitoses, there was no considerable change in nuclear density in any of the single and double deletion mutants analyzed here under low-density conditions. We would expect that elimination of local control of mitosis might be globally reflected in the average nuclear distance. The fact that this is not the case suggests the existence of redundant mechanisms to regulate nuclear division rate. Loss of local stimulation of mitosis at branching sites could be compensated for by yet unidentified ways to decrease AgSwe1p activity in a more global manner, coupled with efficient migration and distribution of nuclei along microtubules (Alberti-Segui *et al.*, 2001). Notably, such potential mechanisms of compensation can be bypassed or suppressed by overexpressing Ag*SWE1* from the Sc*HIS3* promoter, which results in decreased nuclear density even under rich nutrient conditions. One way to explain this is that AgSwe1p activity could globally be restricted on a transcriptional level in addition to being locally controlled by protein inhibition/degradation. This transcriptional control would no longer be functional when AgSwe1p is expressed from an exogenous promoter.

Although it is still unclear how AgSwe1p influences the position of mitotic progression in the presence of abundant nutrients, we present evidence that AgSwe1p does phosphorylate and inhibit AgCdc28p and pause nuclear division under starvation signals, even when hyphal growth continues. We observed that AgCdc28p is phosphorylated on the Y18 residue in high-density growth or conditions that mimic starvation, and this is correlated with an accumulation of nuclei with duplicated SPBs and metaphase spindles and a decreased nuclear density (Figure 8D). Overexpression of AgSwe1p is sufficient to induce some changes to the nuclear division cycle, the delay in G2, even without nutrient deprivation. Interestingly, the AgSwe1p-dependent response to low nutrients was exacerbated in cells lacking septins or cells in which the septins have been deleted in combination with the phosphatase, AgMih1p, which likely removes the Y18 phosphorylation. This suggests that the septins may regulate the AgSwe1p-dependent response to nutrient status. Alternatively or additionally, this AgSwe1p response could also be spatially controlled by clustering of receptors/signaling factors for sensing nutrient status on the cell surface, which then inactivate a pool of AgSwe1p to generate mitoses locally.

Surprisingly, a complete nuclear arrest was never observed even when both the putative AgSwe1p inhibitor AgHsl1p and the phosphatase AgMih1p are deleted. This is in clear contrast to budding yeast, where double deletion of ScMih1p and ScHsl1p leads to a lethal arrest at the G2-M transition (McMillan *et al.*, 1999a). Conceivably, some portion of the CDK pool is shielded from interaction with AgSwe1p so that a uniform arrest does not take place. For example, some nuclei could block nuclear import of AgSwe1p and AgCdc28p in these nuclei would no longer be accessible for AgSwe1p-mediated inhibition, enabling such nuclei to divide independently of the levels of active AgSwe1p. Alternatively, Y18 phosphorylation of AgCdc28p could only partially inhibit activity of the CDK in *A. gossypii.*

How might AgSwe1p activity be enhanced by nutrient limitation? In budding yeast cells, ScSwe1p participates in the filamentous differentiation response to nutrient limitation through inhibiting CDK/Clb2 complexes, which extends G2 and promotes hyperpolarized bud growth (Edgington *et al.*, 1999; La Valle and Wittenberg, 2001). It is unclear, however, how the status of environmental conditions is transmitted to ScSwe1p and its regulators that are partially responsible for sustaining this differentiation program. Both the STE MAPK and the RAS/cAMP pathways have known "anchors" at the plasma membrane sensor level and the nuclear transcriptional response level; however, ScSwe1p can act independently of these pathways in filamentation (Ahn *et al.*, 1999). How Swe1p senses nutrient status in budding yeast is unknown. In fission yeast, nutrient limitation signals through a MAP kinase called Spc1 and triggers a Wee1-mediated G2 delay potentially through the regulation of nim1 (Shiozaki and Russell, 1995; Belenguer *et al.*, 1997). *A. gossypii* is constitutively filamentous, and unlike in *S. cerevisiae* strains, filamentous morphology changes are not observed under nutrient deprivation. Nevertheless, AgSwe1p activity makes dramatic contributions to the nuclear division cycle kinetics in starving *A. gossypii* cells. It was remarkable that inhibition of AgTor1/2p by rapamycin could activate AgSwe1p similarly to nutrient deprivation, suggesting that AgSwe1p activity in response to starvation may be regulated downstream of this master regulator of cell growth. This Tor1/2p path and/or a MAPK/RAS/cAMP path could communicate nutrient status and influence AgSwe1p in a variety of ways either by influencing its stability, its localization, its transcription, or its intrinsic kinase activity or affinity for AgCdc28p. Future work will be aimed at understanding how this conserved kinase senses and responds to nutrient fluctuations.

Filamentous fungi inhabit heterogenous environments in the natural world. There is spatial and temporal irregularity

in many factors such as water, temperature, minerals, and pH, in addition to carbon and nitrogen sources. *A. gossypii* is found outside the laboratory as a tropical plant pathogen where it is transmitted by sucking insects and can infect cotton and citrus fruits leading to dry rot (Ashby, 1926; Batra, 1973). Given the large potential size of a filamentous fungal mycelium in which many interconnected hyphae share a common cytoplasm, a single cell may simultaneously experience "feast and famine" conditions. In some fungi, branching is induced by exposure to pockets of nutrients, allowing the cell to forage and exploit that presumably limited source (Ritz, 1995). A cell would ideally target these resources locally, producing more nuclei to support the exploring hyphae, while the rest of the nuclei and cell remain quiescent. In a syncytium, however, it is unclear how a cell may delineate the active and inactive regions. Our current laboratory culturing conditions of *A. gossypii* make it difficult to simulate the nutrient heterogeneity such cells would encounter in the natural world. However, we have attempted to integrate the data we have generated on AgSwe1p spatially directing mitosis in the presence of abundant nutrients and AgSwe1p inhibiting mitosis during starvation into a model. We envision testing this model once more heterogeneous environmental conditions can be replicated in the laboratory. We speculate that septins and AgSwe1p may function to locally generate nuclei in a region of the cell experiencing a limited surplus of nutrients. In this model, sudden increases in the pools of nutrients would lead to local assembly of a septin ring, branch initiation, and perhaps activation of the TOR pathway, which may then promote mitoses in this limited area through the inactivation of AgSwe1p locally (Figure 8E). Future studies will examine this novel role of AgSwe1p and septins for influencing the position of mitoses in multinucleated cells.

ACKNOWLEDGMENTS

We thank Danny Lew, Kelly Tatchel, Hans-Peter Schmitz, Peter Philippsen, Jake Harrison, and Chandra Theesfeld for critically reading the manuscript. We are grateful to Mark Borsuk for consultation about statistical analysis of the data. We are indebted to Peter Philippsen for constant encouragement of this work and for conceiving of the diagram used in Figure 1. This work was supported by an National Science Foundation postdoctoral fellowship, a Roche Research Foundation fellowship, and a Swiss National Fund Grant (3100A0-100734) to Peter Philippsen and A.S.G.

REFERENCES

Ahn, S. H., Acurio, A., and Kron, S. J. (1999). Regulation of G2/M Progression by the STE mitogen-activated protein kinase pathway in budding yeast filamentous growth. Mol. Biol. Cell *10*, 3301–3316.

Alberti-Segui, C., Dietrich, F., Altmann-Johl, R., Hœpfner, D., and Philippsen, P. (2001). Cytoplasmic dynein is required to oppose the force that moves nuclei towards the hyphal tip in the filamentous ascomycete *Ashbya gossypii*. J. Cell Sci. *114*, 975–986.

Altmann-Johl, R., and Philippsen, P. (1996). AgTHR4, a new selection marker for transformation of the filamentous fungus *Ashbya gossypii*, maps in a four-gene cluster that is conserved between *A. gossypii* and *Saccharomyces cerevisiae*. Mol. Gen. Genet. *250*, 69–80.

Arvanitidis, A., and Heinisch, J. J. (1994). Studies on the function of yeast phosphofructokinase subunits by in vitro mutagenesis. J. Biol. Chem. *269*, 8911–8918.

Asano, S., Park, J. E., Sakchaisri, K., Yu, L. R., Song, S., Supavilai, P., Veenstra, T. D., and Lee, K.S. (2005). Concerted mechanism of Swe1/Wee1 regulation by multiple kinases in budding yeast. EMBO J. *24*, 2194–2204.

Ashby, S., and Nowell, W. (1926). The fungi of stigmatomycosis. Ann. Botany *40*, 69–84.

Ayad-Durieux, Y., Knechtle, P., Goff, S., Dietrich, F., and Philippsen, P. (2000). A PAK-like protein kinase is required for maturation of young hyphae and septation in the filamentous ascomycete *Ashbya gossypii*. J. Cell Sci. *113*(Pt 24), 4563–4575.

Barral, Y., Parra, M., Bidlingmaier, S., and Snyder, M. (1999). Nim1-related kinases coordinate cell cycle progression with the organization of the peripheral cytoskeleton in yeast. Genes Dev. *13*, 176–187.

Batra, L. R. (1973). Nematosporaceae (Hemiascomycetidae): taxonomy, pathogenicity, distribution, and vector relations. USDA Tech. Bull. *1469*, 1–71.

Baudin, A., Ozier-Kalogeropoulos, O., Denouel, A., Lacroute, F., and Cullin, C. (1993). A simple and efficient method for direct gene deletion in *Saccharomyces cerevisiae*. Nucleic Acids Res. *21*, 3329–3330.

Belenguer, P., Pelloquin, L., Oustrin, M. L., and Ducommun, B. (1997). Role of the fission yeast nim 1 protein kinase in the cell cycle response to nutritional signals. Biochem. Biophys. Res. Commun. *232*, 204–208.

Cid, V. J., Shulewitz, M. J., McDonald, K. L., and Thorner, J. (2001). Dynamic localization of the Swe1 regulator Hsl7 during the *Saccharomyces cerevisiae* cell cycle. Mol. Biol. Cell *12*, 1645–1669.

Clutterbuck, A. J. (1970). Synchronous nuclear division and septation in *Aspergillus nidulans*. J. Gen. Microbiol. *60*, 133–135.

Dietrich, F. S., *et al*. (2004). The *Ashbya gossypii* genome as a tool for mapping the ancient *Saccharomyces cerevisiae* genome. Science *304*, 304–307.

Douglas, L. M., Alvarez, F. J., McCreary, C., and Konopka, J. B. (2005). Septin function in yeast model systems and pathogenic fungi. Eukaryot. Cell *4*, 1503–1512.

Edgington, N. P., Blacketer, M. J., Bierwagen, T. A., and Myers, A. M. (1999). Control of *Saccharomyces cerevisiae* filamentous growth by cyclin-dependent kinase Cdc28. Mol. Cell. Biol. *19*, 1369–1380.

Entian, K., and Koetter, P. (1998). Yeast mutant and plasmid collections. In: Methods in Microbiology, Vol. 26, ed. A.J.P. Brown and M. Tuite, San Diego: Academic Press, 431–449.

Freitag, M., Hickey, P. C., Raju, N. B., Selker, E. U., and Read, N. D. (2004). GFP as a tool to analyze the organization, dynamics and function of nuclei and microtubules in *Neurospora crassa*. Fungal Genet. Biol. *41*, 897–910.

Gladfelter, A. S. (2006). Control of filamentous fungal cell shape by septins and formins. Nat. Rev. Microbiol. *4*, 223–229.

Gladfelter, A. S., Hungerbuehler, A. K., and Philippsen, P. (2006). Asynchronous nuclear division cycles in multinucleated cells. J. Cell Biol. *172*, 347–362.

Gladfelter, A. S., Pringle, J. R., and Lew, D. J. (2001). The septin cortex at the yeast mother-bud neck. Curr. Opin. Microbiol. *4*, 681–689.

Hanahan, D. (1983). Studies on transformation of *Escherichia coli* with plasmids. J. Mol. Biol. *166*, 557–580.

Harris, S. D., and Momany, M. (2004). Polarity in filamentous fungi: moving beyond the yeast paradigm. Fungal Genet. Biol. *41*, 391–400.

Hœpfner, D., Brachat, A., and Philippsen, P. (2000). Time-lapse video microscopy analysis reveals astral microtubule detachment in the yeast spindle pole mutant cnm67. Mol. Biol. Cell *11*, 1197–1211.

Kellogg, D. R. (2003). Wee1-dependent mechanisms required for coordination of cell growth and cell division. J. Cell Sci. *116*, 4883–4890.

Knechtle, P., Dietrich, F., and Philippsen, P. (2003). Maximal polar growth potential depends on the polarisome component AgSpa2 in the filamentous fungus *Ashbya gossypii*. Mol. Biol. Cell *14*, 4140–4154.

La Valle, R., and Wittenberg, C. (2001). A role for the Swe1 checkpoint kinase during filamentous growth of *Saccharomyces cerevisiae*. Genetics *158*, 549–562.

Lew, D. J. (2003). The morphogenesis checkpoint: how yeast cells watch their figures. Curr. Opin. Cell Biol. *15*, 648–653.

Loewith, R., Jacinto, E., Wullschleger, S., Lorberg, A., Crespo, J. L., Bonenfant, D., Oppliger, W., Jenoe, P., and Hall, M. N. (2002). Two TOR complexes, only one of which is rapamycin sensitive, have distinct roles in cell growth control. Mol. Cell *10*, 457–468.

Longtine, M. S., and Bi, E. (2003). Regulation of septin organization and function in yeast. Trends Cell Biol. *13*, 403–409.

Longtine, M. S., Theesfeld, C. L., McMillan, J. N., Weaver, E., Pringle, J. R., and Lew, D. J. (2000). Septin-dependent assembly of a cell-cycle-regulatory module in *Saccharomyces cerevisiae*. Mol. Cell. Biol. *20*, 4049–4061.

Martin, D. E., and Hall, M. N. (2005). The expanding TOR signaling network. Curr. Opin. Cell Biol. *17*, 158–166.

McElver, J., and Weber, S. (1992). Flag N-terminal epitope overexpression of bacterial alkaline phosphatase and Flag C-terminal epitope tagging by PCR one-step targeted integration. Yeast 8(special issue), S627.

McMillan, J. N., Longtine, M. S., Sia, R. A., Theesfeld, C. L., Bardes, E. S., Pringle, J. R., and Lew, D. J. (1999a). The morphogenesis checkpoint in

Saccharomyces cerevisiae: cell cycle control of Swe1p degradation by Hsl1p and Hsl7p. Mol. Cell. Biol. *19*, 6929–6939.

McMillan, J. N., Sia, R.A.L., Bardes, E.S.G., and Lew, D. J. (1999b). Phosphorylation-independent inhibition of Cdc28p by the tyrosine kinase Swe1p in the morphogenesis checkpoint. Mol. Cell. Biol. *19*, 5981–5990.

McMillan, J. N., Sia, R.A.L., and Lew, D. J. (1998). A morphogenesis checkpoint monitors the actin cytoskeleton in yeast. J. Cell Biol. *142*, 1487–1499.

Minke, P. F., Lee, I. H., and Plamann, M. (1999). Microscopic analysis of *Neurospora* ropy mutants defective in nuclear distribution. Fungal Genet Biol. *28*, 55–67.

Nygaard, O. F., Guttes, S., and Rusch, H. P. (1960). Nucleic acid metabolism in a slime mold with synchronous mitosis. Biochim. Biophys. Acta *38*, 298–306.

Ritz, K. (1995). Growth response of some soil fungi to spatially heterogenous nutrients. FEMS Microbiol. Ecol. *16*, 269–280.

Sakchaisri, K., Asano, S., Yu, L. R., Shulewitz, M. J., Park, C. J., Park, J. E., Cho, Y. W., Veenstra, T. D., Thorner, J., and Lee, K. S. (2004). Coupling morphogenesis to mitotic entry. Proc. Natl. Acad. Sci. USA *101*, 4124–4129.

Sambrook, J.a.D.R. (2001). Molecular Cloning: A Laboratory Manual, Cold Spring Harbor Laboratory Press: Cold Spring Harbor.

Schmitz, H. P., Kaufmann, A., Kohli, M., Laissue, P. P., and Philippsen, P. (2006). From function to shape: a novel role of a formin in morphogenesis of the fungus *Ashbya gossypii.* Mol. Biol. Cell *17*, 130–145.

Shiozaki, K., and Russell, P. (1995). Cell-cycle control linked to extracellular environment by MAP kinase pathway in fission yeast. Nature *378*, 739–743.

Shulewitz, M. J., Inouye, C. J., and Thorner, J. (1999). Hsl7 localizes to a septin ring and serves as an adapter in a regulatory pathway that relieves tyrosine phosphorylation of Cdc28 protein kinase in *Saccharomyces cerevisiae.* Mol. Cell. Biol. *19*, 7123–7137.

Sia, R.A.L., Bardes, E.S.G., and Lew, D. J. (1998). Control of Swe1p degradation by the morphogenesis checkpoint. EMBO J. *17*, 6678–6688.

Sia, R.A.L., Herald, H. A., and Lew, D. J. (1996). Cdc28 tyrosine phosphorylation and the morphogenesis checkpoint in budding yeast. Mol. Biol. Cell *7*, 1657–1666.

Sikorski, R. S., and Hieter, P. (1989). A system of shuttle vectors and yeast host strains designed for efficient manipulation of DNA in *Saccharomyces cerevisiae.* Genetics *122*, 19–27.

Wach, A. (1996). PCR-synthesis of marker cassettes with long flanking homology regions for gene disruptions in *S. cerevisiae.* Yeast *12*, 259–265.

Wendland, J., Ayad-Durieux, Y., Knechtle, P., Rebischung, C., and Philippsen, P. (2000). PCR-based gene targeting in the filamentous fungus *Ashbya gossypii.* Gene *242*, 381–391.

Westfall, P. J., and Momany, M. (2002). *Aspergillus nidulans* septin AspB plays pre- and postmitotic roles in septum, branch, and conidiophore development. Mol. Biol. Cell *13*, 110–118.